Ragweed pollen production and dispersion modelling within a regional climate system, calibration and application over Europe

L. Liu[1, 2], F. Solmon[1], R. Vautard[3], L. Hamaoui-Laguel[3, 4], Cs. Zs. Torma[1], and F. Giorgi[1]

[1]{Earth System Physics Section, the Abdus Salam International Centre for Theoretical Physic, Trieste, Italy}

[2]{Guizhou Key Laboratory of Mountainous Climate and Resources, Guiyang, China}

[3]{Laboratoire des Sciences du Climat et de l'Environnement, IPSL, CEA-CNRS-UVSQ, UMR8212, Gif sur Yvette, France}

[4]{Institut National de l'Environnement Industriel et des Risques, Parc technologique ALATA, Verneuil en Halatte, France}

Correspondence to: L. Liu (liliuliulish@outlook.com); F. Solmon (fsolmon@ictp.it)

1   **Abstract**

2   Common ragweed (*Ambrosia artemisiifolia L.*) is a highly allergenic and invasive plant in
3   Europe. Its pollen can be transported over large distances and has been recognized as a
4   significant cause of hayfever and asthma (D'Amato et al., 2007; Burbach et al., 2009). To
5   simulate production and dispersion of common ragweed pollen, we implement a pollen
6   emission and transport module in the Regional Climate Model (RegCM) version 4 using the
7   framework of the Community Land Model (CLM) version 4.5. In this on line approach pollen
8   emissions are calculated based on the modelling of plant distribution, pollen production,
9   species-specific phenology, flowering probability, and flux response to meteorological
10   conditions. A pollen tracer model is used to describe pollen advective transport, turbulent
11   mixing, dry and wet deposition.

12   The model is then applied and evaluated on a European domain for the period 2000-2010. To
13   reduce the large uncertainties notably due to the lack of information on ragweed density
14   distribution, a calibration based on airborne pollen observations is used. Accordingly a cross
15   validation is conducted and shows reasonable error and sensitivity of the calibration.
16   Resulting simulations show that the model captures the gross features of the pollen
17   concentrations found in Europe, and reproduce reasonably both the spatial and temporal
18   patterns of flowering season and associated pollen concentrations measured over Europe. The
19   model can explain 68.6%, 39.2%, and 34.3% of the observed variance in starting, central, and
20   ending dates of the pollen season with associated root mean square error (RMSE) equal to 4.7,
21   3.9, and 7.0 days, respectively. The correlation between simulated and observed daily
22   concentrations time series reaches 0.69. Statistical scores show that the model performs better
23   over the central Europe source region where pollen loads are larger and the model is better
24   constrained..

25   From these simulations health risks associated to common ragweed pollen spread are
26   evaluated through calculation of exposure time above health-relevant threshold levels. The
27   total risk area with concentration above 5 grains m^{-3} takes up 29.5% of domain. The longest
28   exposure time occurs on Pannonian Plain, where the number of days per year with the daily
29   concentration above 20 grains m^{-3} exceeds 30.

30

31

1 Introduction

Ambrosia artemisiifolia L. (common ragweed, hereafter ragweed), is an alien plant that has invaded parts of Europe over the last century, creating severe allergies in populations (Chauvel et al., 2006; Kazinczi et al., 2008; Gallinza et al., 2010; Pinke et al., 2011). It has been shown that concentrations of ragweed pollen down to 5-10 grains m^{-3} can lead to health problems for sensitive persons (Taramarcaz et al., 2005). In Europe, ragweed typically flowers from July to October (Kazinczi et al., 2008). Ragweed has developed wind pollination strategy, which allows each plant to produce millions of pollen grains with diameter of 18-22 μm and containing small air chambers (Payne, 1963). Pollen grains can readily become airborne when conditions are favourable (Dahl et al., 1999; Taramarcaz et al., 2005; Cecchi et al., 2006; Stach et al., 2007; Smith et al., 2008; Šikoparija et al., 2013).

One of the goals of the project "Atopic diseases in changing climate, land use and air quality" (ATOPICA) (http://www.atopica.eu) is to better understand and quantify the effects of environmental changes on ragweed pollen and associated health impacts over Europe. In this context the present study introduces a modelling framework designed to simulate production and dispersion of ragweed pollen. Ultimately these models can be used for investigating the effects of changing climate and land use on ragweed (Hamaoui-Laguel et al., 2015) and for providing relevant data to health impact investigators.

Presently a number of regional models, mostly designed for air quality prevision, incorporate release and dispersion dynamics of pollen (Helbig et al., 2004; Sofiev et al., 2006; Skjøth, 2009; Efstathiou et al., 2011; Zink et al., 2012; Prank et al., 2013; Sofiev et al., 2013; Zhang et al., 2014). Methods for producing ragweed pollen emission suitable for input to regional scale models have been developed in recent studies (Skjøth et al., 2010; Šikoparija et al., 2012; Chapman et al., 2014). Due to lack of statistical information related to plant location and amount within a given geographical area, the bottom up approach to produce plant presence inventories is unpractical for most herbaceous allergenic species like ragweed. Quantitative habitat maps for such species are often derived from spatial variations in annual pollen sum, knowledge on plant ecology and detailed land cover information by top-down approach (such as Skjøth et at., 2010, Skjøth et al., 2013, Thibaudon et al., 2014, Karrer et al., 2015). Lately, an observation-based habitat map of ragweed has been published in the context of the ENV.B2/ETU/2010/0037 project "Assessing and controlling the spread and the effects of common ragweed in Europe" (Bullock et al., 2012). This inventory is further calibrated

against airborne pollen observations to reproduce the ragweed distribution with a high accuracy, according to Prank et al (2013). Recently Hamaoui-Laguel et al. (2015) used the observations collected in Bullock et al. (2012), combined with simplified assumptions on plant density and a calibration using observations to obtain a ragweed density inventory map. This approach made use of the Organising Carbon and Hydrology in Dynamic Ecosystems (ORCHIDEE) and the Phenological Modeling Platform (PMP) for obtaining daily available pollens (potential emissions) in Europe.

On average, one ragweed plant can produce 1.19 ± 0.14 billion pollen grains in a year (Fumanal et al., 2007), but resources available (solar radiation, water, CO_2, and nutrients) for an individual plant during the growth season could alter its fitness and further influence its pollen production (Rogers et al., 2006; Simard and Benoit, 2011, 2012). Fumanal et al (2007) investigate the individual pollen production of different common ragweed populations in natural environment and propose a quantitative relationship between annual pollen production and plant biomass at the beginning of flowering. This allows to integrate the response of productivity to various environmental conditions through land surface model.

The timing of the emission can be estimated from a combination of phenological models and the species specific pollen release pattern driven by short-term meteorological conditions (Martin et al., 2010; Smith et al., 2013; Zink et al., 2013). Ragweed is a summer annual, short-day plant. Before seeds are able to germinate, it requires a period of chilling to break the dormant state (Willemsen, 1975). The following growth and phenological development depends on both temperature and photoperiod (Allard, 1945; Deen et al., 1998a). Flowering is initiated by a shortening length of day but could be terminated by frost (Dahl et al., 1999; Smith et al., 2013) or drought (Storkey et al., 2014). A number of phenological models have been developed for ragweed, either based on correlation fitting between climate and phenological stages (García-Mozo et al., 2009) or explicitly represented by biological mechanisms (Deen et al., 1998a; Shrestha et al., 1999; Storkey et al., 2014; Chapman et al., 2014). The mechanistic models take into account the responses of development rates to temperature, photoperiod, soil moisture, or stress condition (frost, drought, etc.). Mostly they are based on growth experiments but have to enforce a standard calendar date or a fixed day length for the onset of flowering when they are used in real condition. While the airborne pollen observations from European pollen monitoring sites have a high year to year, site to site variability. Therefore it might be practical to combine the mechanistic model with

correlation fitting when the knowledge of plant physiology and local adaptation of phenology are not sufficiently known at the moment.

In this paper, we present a pollen emission scheme that incorporate plant distribution, pollen production, species-specific phenology, flowering probability distribution, and pollen release based on recent studies. By combining the emission scheme with a transport mechanism a pollen simulation framework within the Regional Climate Model (RegCM) version 4 is then developed to study ragweed pollen dispersion behaviours on regional scale. In Sect. 2 we provide a description of the RegCM-pollen simulation configuration, emission parameterization details, the processing of plant spatial density and observations data used for calibration in the study. In Sect 3 we define the model experiment, explain the method used to calibrate ragweed density, present the simulation results of pollen season, evaluate the performances of the coupled model system over a recent period covered with observations, and finnaly present the climatological information about the ragweed pollen risk over European domain on decadal time scale. Summary and conclusions appear in Sect. 4.

2   Materials and methods

The development of RegCM-pollen model is based on the Abdus Salam International Centre for Theoretical Physics (ICTP) regional climate model, i.e. RegCM4, which has been used for a number of years in a wide variety of applications (Giorgi et al., 2006; Meleux et al., 2007; Pal et al., 2007; Giorgi et al., 2012). In this framework, we develop a pollen model for ragweed which calculates (i) the seasonal production of pollen grains and (ii) their emission and atmospheric processes (transport and deposition) determining regional pollen concentrations. As detailed hereafter pollen emission and transport are developed in the preexisting framework of the RegCM atmospheric chemistry module (Solmon et al., 2006; Zakey et al., 2006; Tummon et al., 2010; Shalaby et al., 2012; Solmon et al., 2012). Pollen production is developed in the framework of the Community Land Model (CLM) version 4.5 (Oleson et al., 2013), which is the land surface scheme coupled to RegCM. Figure 1 gives an overview of such development framework. In the following subsections, we give details about the important data and steps of the development.

2.1   Observed pollen concentrations

Pollen observations are central for calibration and validation of the pollen module as discussed further. The pollen data are provided by the European Aeroallergen Network

1 (https://ean.polleninfo.eu/Ean/) and affiliated national aerobiology monitoring network

2 RNSA(France, http://www.pollen.fr), ARPA-Veneto (Italy, http://www.arpa.veneto.it), and

3 Croatian organizations including the Institute of Public Health, the Department of

4 Environmental Protection and Health Ecology at Institute of Public Health "Andrija Štampar"

5 and Associate-degree college of Velika Gorica. The archives cover ragweed pollen

6 concentrations (expressed as grain·m^{-3}) with daily resolution from 44 observations stations

7 from 2000 to 2012 year (Table 1). The pollen observation sites range from 42.649°N to

8 48.300°N and from 0.164°E to 21.583°E. The sites are grouped for study purposes into four

9 regions: France (FR), Italy (IT), Germany-Switzerland (DE+CH) and central Europe (Central

10 EU) including Austria, Croatia, and Hungary (Fig. 2). Ragweed pollens are collected at an

11 airflow rate of 10 L min^{-1} using volumetric spore traps based on the Hirst (1952) design.

12 Samples were examined with light microscopy for the identification and counting of pollen

13 grains. The International Association for Aerobiology recommends for the samples reading at

14 magnification 400x minimum of 3 longitudinal bands or at least 12 transverse bands or

15 minimum 500 random fields (Jäger et al., 1995). The actual sampling methods (longitudinal,

16 transverse or random) and magnifications may vary between the several national networks but

17 generally comply (Jato et al., 2006; Skjøth et al., 2010; García-Mozo et al., 2009; Sofiev et al.,

18 2015; Galán et al., 2014; Thibaudon et al., 2014). We based our study on daily pollen

19 concentrations, although for some stations hourly data are available. The observations period

20 ranges from 2000 to 2012 but for some stations observations only cover part of this period.

21 The observations of 2000-2010 are designed for model application and evaluation about

22 ragweed pollen risk. The data for 2011 and 2012 are left and only used for verifing pollen

23 season simulated by phenology model.

24 **2.2 Model setup**

25 Ragweed pollen simulations are carried out for a European domain ranging from

26 approximately 35°N to 70°N, and from 20°W to 40°E (Fig. 2). The horizontal resolution is 50

27 km, with 23 atmospheric layers from the surface to 50 hPa. Initial and lateral atmospheric

28 boundary conditions are provided by ERA-Interim analysis at 1.5°spatial resolution and 6-h

29 temporal resolution. Weekly SSTs are obtained from the NOAA optimum interpolation (OI)

30 SST analysis (with weekly ERA sea surface temperatures). Beside CLM4.5 as a land surface

31 scheme, other important physical options are Holtslag PBL scheme (Holtslag et al., 1990) for

32 boundary layer, Grell scheme (Grell, 1993) over land and Emanuel scheme (Emanuel and

1 Zivkovic-Rothman, 1999) over ocean for convective precipitation, the SUBEX scheme (Pal et

2 al., 2000) for large-scale precipitation. Aerosol and humidity are advected using a semi-

3 Lagrangian scheme. The period 2000-2010 is chosen for the study. Even though the focus of

4 the study is July-October of the flowering season, the model is integrated continuously

5 throughout the year notably for simulating ragweed phenology. To compare with the

6 observation described in Sect. 2.1, simulated pollen concentrations time series are interpolated

7 to the station locations and averaged daily.

8 2.3 Ragweed spatial density

9 Ragweed spatial distribution is obtained through a procedure discussed in Hamaoui-Laguel et

10 al. (2015) (Supplementary Information). For country where observations are available and of

11 sufficient quality, ragweed distribution is assumed to result from habitat suitability combined

12 with infestation (not all suitable habitats are populated). The habitat suitability is assumed to

13 scale as the product of the fraction of suitable land use surface *H(x,y)* with a climate

14 suitability index *CI(x,y)* calculated from the SIRIUS ecological model (Storkey et al., 2014).

15 The infestation rate is derived from the density of 10×10 km cells *K(x,y)* with plant presence

16 as reported in Bullock et al. (2012). Assuming a homogeneous surface distribution of suitable

17 habitats within each model grid cell (50x50 km) and assuming that observers only investigate

18 suitable areas, the probability of plant presence (or infestation rate) should then be

19 proportional to *K(x,y)/25*. But considering that an observer probably finds ragweed plants

20 more often than what a random search would predict, the density should actually be lower

21 than that predicted by *K(x,y)/25*. We assumed that infestation rate actually scales as

22 $(K(x,y)/25)^r$, with *r>1*, taken here equals to 2. The final ragweed density D_p (in plant·m^{-2}) at

23 50 km resolution is therefore obtained from the infestation rate, surface fraction of suitable

24 land use, and climatic suitability index as:

$$25 \qquad D_p(x,y) = Const \cdot H(x,y) \cdot CI(x,y) \cdot (\frac{K(x,y)}{25})^r \qquad , \qquad (1)$$

26

27 Here *Const = 0.02* is assumed to be the maximal density (plant·m^{-2}) in the most suitable

28 habitats (Efstathiou et al., 2011), *H(x,y)* taken as the crop and urban lands in CMIP5 land use

29 classification (Hurtt et al., 2006). For countries with low-quality observations or with no

30 available inventories, the detection probability is replaced by the average over neighbouring

31 countries with reliable data.

2.4 Parameterization of the pollen emission flux

Pollen emission patterns on regional scale depend on plant density, production, and meteorological conditions. The parameterization of pollen emission flux is a modified version of Helbig et al. (2004). The vertical flux of pollen particles F_p in a given grid cell is assumed to be proportional to the product of a characteristic pollen grain concentration per plant individual c^* (grain·m^{-3}·plant^{-1}) and the local friction velocity u_*. This potential flux is then modulated by a plant-specific factor c_e that describes the likelihood of blossoming, and a meteorological adjustment factor. Finally the flux is scaled up at the grid level using the plant density D_p (plant·m^{-2}) discussed previously in Sect. 2.3.

$$F_p = D_p.c_e.K_e.c^*.u_* \qquad , \qquad (2)$$

2.5 Pollen production

The characteristic concentration c^* is related to pollen grain production using

$$c^* = \frac{q_p}{LAI \cdot H_s} \qquad , \qquad (3)$$

where q_p is the annual pollen production in grains per individual plant (grains·plant^{-1}), $LAI=3$ is the leaf area index term, and $H_s =1$ is the canopy height (m). These later parameter are determined on the basis of CLM4.5 C3 grass land use categories during summer.

Annual pollen production q_p is estimated from plant biomass production, based on an assumption that pollen production per plant is a function of the plant dry biomass i.e. the accumulated net primary production (NPP) of CLM4.5 C3 grass plant functional type during the growth season. Based on this assumption, q_p is calculated following Fumanal et al. (2007) (Eq. 4). This parameterisation integrates the response of pollen grain productivity to various environmental conditions affecting C3 grass NPP, including climate variables and atmospheric CO_2 concentration for example. It involves a variety of biophysical and biogeochemical processes at the surface such as photosynthesis, phenology, allocation of carbon/nitrogen assimilates in the different components of plant, biomass turnover, litter decomposition, and soil carbon/nitrogen dynamics.

$$Log_{10}(q_p) = 7.22 + 1.12 \log_{10}(plant \ \ dry \ \ biomass) \qquad , \qquad (4)$$

1 In this approach, yearly total pollen production calculation from mature plant dry biomass

2 needs to be determined in advance, i.e. before integration of the pollen modelling chain. This

3 is done by making a preliminary RegCM-CLM4.5 run with prognostic NPP activated and

4 archived. Alternatively, in order to reduce simulation costs and insure model portability to

5 other domain we also built a precomputed global C3 grass yearly accumulated NPP data base.

6 This data can be directly interpolated and prescribed to RegCM4 for pollen runs. This global

7 data base is built by running the land component CLM4.5 of the Community Earth System

8 Model version 1.2 (CESM1.2) (Oleson et al., 2013) with the Biome-BGC biogeochemical

9 model (Thornton et al., 2002; Thornton et al., 2007) enabled and forced by CRUNCEP

10 (Viovy, 2011). We acknowledge that NPP obtained this way is not fully consistent with

11 RegCM simulated climate but this approach represents a reasonable and practical compromise.

12 **2.6 Flowering probability density distribution**

13 In Eq. (2), C_e is a probability density function accounting for the likelihood of the plant to

14 flower and effectively release pollen in the atmosphere. The inflorescences of common

15 ragweed consist of many individual flowers that reach anthesis sequentially (Payne, 1963). At

16 the beginning of the season only a few plants flower and the amount of available pollen grains

17 is small, regardless of the favourable meteorological conditions. The number of flowers

18 increases with time until a maximum is reached. Afterwards, the number decreases again until

19 the end of the pollen season. To represent this dynamic, we use the normal distribution

20 function reported in Prank et al. (2013). The probability distribution of flowering time is

21 represented by a Gaussian depending on "accumulated biological days" BD, and centred

22 midway between flowering starting and ending biological days BD_{fe} and BD_{fs}:

23
$$c_e = const \cdot \frac{1}{\sigma\sqrt{2\pi}} \cdot e^{-\frac{(BD - \frac{BD_{fe} + BD_{fs}}{2})^2}{2\sigma^2}}$$

24
, $\qquad$ (5)

25 where $const = 20 \cdot 10^{-4}$ is determined by adjusting the integrated amount of pollens between

26 BD_{fe} and BD_{fs} to the total yearly production q_p determined from NPP. σ is the standard

27 deviation determined by the length of the season, considering that the season represents about

28 four standard deviations of the Gaussian distribution $4\sigma = BD_{fe} - BD_{fs}$. The probability

29 distribution is however set to zero as soon as the daily minimum temperature is below $0\,^{\circ}\mathrm{C}$,

1 considering that first frost set up the end of ragweed activity (Dahl et al., 1999). In the

2 following section we describe how biological days (BD) are effectively determined.

2.7 Phenology representation and flowering season definition

2.7.1 Biological days

5 For simulating the timing of the flowering season, we adapt the mechanistic phenology

6 model of Chapman et al. (2014), which is based on growth experiments (Deen et al., 1998a;

7 Deen et al., 1998b; Shrestha et al., 1999; Deen et al., 2001). Phenology is simulated using

8 BD accumulated for the current year of simulation and from the first day (t_0) after the

9 spring equinox for which daily minimum temperature exceeds a certain threshold T_{min}

10 defined further (Chapman et al., 2014). *BD* on time t depends on key environmental

11 variables through:

12

$$BD(T, L, \theta) = \int_{t_0} r_T(T) \cdot r_L(L) \cdot r_S(\theta) \cdot dt$$

13   ,   (6)

14 where r_T, r_L, r_S are the response of development rates to temperature T, photoperiod L, and

15 soil moisture θ, respectively. In this approach, biological day varies according to local

16 climate as illustrated in Sect. 3.2. The phenological development of ragweed before flowering

17 is separated into vegetative and reproductive phases controlled by different factors.

18 Vegetative development stages are germination to seedling emergence (4.5 BD) and

19 emergence to end of juvenile phase (7.0 BD) (Deen et al., 2001). The development rate at the

20 germination to seedling emergence is assumed to be affected by temperature and soil moisture,

21 while the rate at the emergence to end of juvenile phase is affected by temperature alone.

22 From the end of the juvenile phase to the beginning of anthesis (13.5 BD) (Deen et al., 2001)

23 the reproductive development phase takes place and is affected by temperature and

24 photoperiod. Vegetative and reproductive processes are assumed to have an identical response

25 to temperature based on the cardinal temperature determined by Chapman et al. (2014)

1
$$r_T(T) = \begin{cases} 0 & T < T_{min} \\ \left(\dfrac{T - T_{min}}{T_{opt} - T_{min}} \left(\dfrac{T_{max} - T}{T_{max} - T_{opt}} \right)^{\frac{T_{max} - T_{opt}}{T_{opt} - T_{min}}} \right)^c & T_{min} \le T \le T_{max} \\ 0 & T > T_{max} \end{cases}$$

,   (7)

2   where T_{min}, T_{opt}, T_{max} are minimum, optimum, and maximum growing temperatures with

3   values 4.88℃, 30.65℃, 42.92℃ respectively. c is a scaling parameter with value of 1.696.

4   All these parameters are derived from growth trail data (Deen et al., 1998a; Deen et al., 1998b;

5   Shrestha et al., 1999; Deen et al., 2001).

6   The response of development rates to photoperiod is simulated using a modified version of

7   function presented by Chapman et al. (2014)

8
9
$$r_L(L) = \begin{cases} e^{(L - 14.0)\ln(1 - L_s)} & L \ge 14.0 \\ 1 & L < 14.0 \end{cases}$$

,   (8)

10

11   where L is day length, expressed in hours. The photoperiod response delays plant

12   development when the day is longer than the threshold photoperiod fixed to 14.0 h (Deen et

13   al., 1998b). Ls is a photoperiod sensitivity parameter varying between 0 and 1, which controls

14   development delay and can be adjusted according to sensitivity test to reflect ragweed

15   phenology adapted to local ecological environment. Photoperiods are assumed to affect

16   reproductive development from the end of the juvenile phase.

17   The response of development rates to soil moisture is assumed to occur from the germination

18   to seedling emergence stage. We use a linear function similar to the one used to account for

19   soil moisture impact on biogenic emission activity factor in MEGAN (Guenther et al., 2012)

20
$$r_S(\theta) = \begin{cases} 0 & \theta < \theta_w \\ \dfrac{\theta - \theta_w}{\theta_{opt} - \theta_w} & \theta_w \le \theta \le \theta_1 \\ 1 & \theta > \theta_1 \end{cases}$$

,   (9)

21   where θ is volumetric water content (m^3 m^{-3}), θ_w (m^3 m^{-3}) is wilting point (the soil moisture

22   level below which plants cannot extract water from soil) and θ_{opt} ($= \theta_w + 0.1$, m^3 m^{-3}) is the

1 optimum soil moisture level in the seed zone over which the development rate reaches

2 maximum (Deen et al., 2001).

3 According to this phenology model, a total of about 25 BD are theoretically needed to reach

4 the beginning of pollen season BD_{fs} from the initiation date of BD accumulation. However

5 this model relies on parameters determined from controlled conditions and transposition to

6 natural environment is not straightforward in order to calculate a realistic BD_{fs}. Moreover, the

7 model does not allow to calculate a priori the end of season date BD_{fe} required in Eq. (5).

8 While we do rely on BD to represent the pheonolgical evolution within the season, we

9 however constrain the starting and ending biological days of the season (BD_{fs} and BD_{fe}) based

10 on observations, as explained hereafter.

11 **2.7.2 Dates of the flowering season**

12 Experimentally, pollen season can be defined in a number of ways from observed pollen

13 concentrations and listed for example in Jato et al. (2006). A widely used definition is the

14 period during which a given percentage of the yearly pollen sum is reached. Another

15 definition refers to the period between the first and last day with pollen concentrations

16 exceeding a specific level. Looking at the temporal distribution of observations, particularly

17 long distribution tails can be found in some cases at the beginning and the end of the pollen

18 season, especially in stations where pollen levels are moderate. This makes the definition of

19 pollen season rather imprecise, while it is in general more constrained in areas with high

20 yearly pollen sum. In our approach, we define the start of the pollen season from 44

21 observation stations (described in Sect. 2.1) as: The first day of a series of three days in a

22 weekly window for which the pollen concentrations exceed 5 grains m^{-3}, and after 2.5% of the

23 yearly pollen sum has been reached. The end of the pollen season is defined as: The last day

24 of a series of three days in a weekly window for which the pollen concentrations exceed 5

25 grains m^{-3}, just before reaching 97.5% of the yearly pollen sum. (5 grains m^{-3} is supposed the

26 minimum threshold to induce medically relevant risks). The centre of the pollen season is

27 simply defined as the time when the yearly pollen sum reaches 50%. Kriging method is then

28 used to spatially interpolate pollen season dates determined for each station over the

29 simulation domain. For each grid cell, BD_{fs} and BD_{fm} are determined by simulating and

30 accumulating biological days up to the experimentally defined starting and mid-season dates.

31 Ending season dates is calculated as $2BD_{fm} - BD_{fs}$ according Eq. (5). This methodology

32 requires again a pre-calculation run of RegCM4/CLM4.5 where simulated BD is output in

1 order to be matched with observed season dates for each year. Once this step is achieved,

2 spatially resolved BD_{fs} and BD_{fe} can be obtained by averaging across the years and used to

3 perform the integrated pollen run.

2.8 Instantaneous release factor

5 In Eq. (2), the K_e factor accounts for short term modulation of pollen flux from

6 meteorological conditions. Following Sofiev et al. (2013) K_e is a function of wind speed,

7 relative humidity, and precipitation calculated by RegCM-CLM45 during the run.

$$ K_e = (\frac{h_{max} - h}{h_{max} - h_{min}}) \cdot [f_{max} - \exp(-\frac{U + w_*}{U_{satur}})] \cdot (\frac{p_{max} - p}{p_{max} - p_{min}}) \tag{10} $$

9 In this formula, h and p are relative humidity (%) and precipitation (mm h^{-1}), which do not

10 affect the release until lower thresholds (h_{min}, p_{min}) are reached. After reaching upper

11 thresholds (h_{max}, p_{max}) the pollen release is totally inhibited. U is the interactive 10 m wind

12 speed (m s^{-1}) connected to RegCM prognostic wind and surface roughness, w_* is a convective

13 velocity scale (m s^{-1}), U_{satur} is the saturation wind speed (m s^{-1}), and f_{max} is the maximum

14 value that wind can contribute to the release rate. The definitions of threshold parameters are

15 discussed in detail in sofiev et al., 2013

16

3 Model application and evaluation

3.1 First guess simulation and calibration of the ragweed density

19 A first pollen run is performed using the first guess ragweed density described in Sect. 2 and

20 displayed in Fig. 3a. First guess density map shows maxima of ragweed in the south-east of

21 France, Benelux countries, and central Europe regions. When comparing the resulting field to

22 observation, simulated concentrations obtained with the first guess distribution are generally

23 overestimated over France, Switzerland and Germany, underestimated in parts of central

24 Europe, and have comparable order of magnitude over some Italian and Croatian stations (Fig.

25 4a). These important biases are in large part due to assumptions made in the construction of

26 the first guess plant density distribution. In order to reduce these biases we perform a model

27 calibration by introducing a correction to the first guess ragweed distribution. For each station,

28 calibration coefficients are obtained by minimizing the yearly root mean square error (RMSE)

after constraining the decadal (2000-2010) mean simulated pollen concentration to match the decadal mean observed concentrations (2000-2010) within an admissible value. Calibration coefficients obtained over each station are then interpolated spatially on the domain using ordinary Kriging technique. Then a calibrated simulation using the calibrated density distribution is carried out and repeated several times. After three iterations, the correlation of yearly totals across observation stations increase from 0.23 to 0.98 and the patterns are clustering around the 1:1 line (Fig. 4b).

The final calibrated ragweed distribution (Fig. 3b) shows high density in central Europe including Hungary, Serbia, Bosnia and Herzegovina, Croatia, and western Romania, northern Italy, west France, and also in southern Netherland and northern Belgium. The calibration adjusts the density over all the grid cells with ragweed presence by a factor ranging between 0.1 and 4.4 with an average of 0.98.

To estimate the error and sensitivity of this calibration method to the individual stations we implement a 5-fold cross validation. The 44 sites are randomly divided into 5 groups. 5 calibration experiments are conducted each time with one group left and used for validation respectively. The results of 5 validation groups are then combined to assess the final performance. With this approach a model measurements Pearson correlation of 0.54 is obtained together with a normalized root mean squared error (RESM) of 21% (Fig 4c). Without surprise, this is less than when using the full data sets for calibration. In particular few stations with particularly high concentrations protruding from surrounding sites (for example, ITMAGE and ROUSSILLON) have a large impact on the results of validation. We compared our cross validation (8 or 9 sites left out each time) with three papers about ragweed pollen source estimation over the Pannonian Plain, France and Austria (Skjøth et al., 2010; Thibaudon et al., 2014; Karrer et al., 2015). Their cross validations (one site left out each time) show corresponding correlations of 0.37, 0.25, 0.63 and root mean squared error of 25%, 16% and 3%, respectively. Our results are within this range. We agree that caution should be taken in areas without a decent number of station coverage where the calibration cannot be done.

Note that through correction, other systematic sources of errors possibly affecting the modelling chain might also be implicitly corrected, leading to undesirable error compensations. However, after running additional tests (not shown here), for example varying

1 model dynamical boundary conditions, a relatively small impact on pollen model performance
2 is found when compared to the ragweed density distribution impact.

3.2 Simulation of pollen season

4 The simulated starting dates, central dates, and ending dates of pollen season are averaged
5 from 2000 to 2010 and presented in Fig. 5. The pollen season generally show a positive
6 gradient from the south to the north and from low altitude to high altitude, resulting from the
7 combined effects of temperature, day length, and soil moisture. The starting date varies
8 between 21 July and 8 September. Flowering starts in the central European source regions
9 earlier than in west and north of source regions. The central dates are reached between 1
10 August and 27 September, without noticeable difference between central and west source
11 regions. Flowering ends in the central later than in the west of source regions. The pollen
12 season is longest in the central main source regions.

13 Table 2 lists the statistical correlation between simulated and observed ragweed pollen
14 starting, central, and ending dates. The model can reproduce starting and central dates better
15 than ending dates. Goodness-of-fit tests show that the models account for 68.6%, 39.2%, and
16 34.3% of the observed variance in starting, central, and ending dates. The RMSE is 4.7, 3.9,
17 and 7.0 days for the pollen starting, central, and ending dates, respectively. The model
18 reproduces the pollen season in the main source regions fairly well (Table 1), where the
19 averaged differences between the simulated and observed pollen season progression are less
20 or equal to 3 days and RMSE is lower than 6 days. For the areas with lower ragweed
21 infestation the results vary widely. The starting dates and central dates are still reproduced
22 well for a majority of the stations while the ending dates are more problematic with averaged
23 differences above 6-10 days and RMSE over 8-12 days at some stations. This might result
24 from patchy local ragweed distribution and the effect of long range transport of pollen, which
25 contributes to the determination of pollen season dates and are assumed to be representative
26 of local flowering in our approach. Some stations also stop pollen measurement before the
27 actual end of pollen season which leads to a lower accuracy of season ending date.

28 This phenology model is further tested for years of 2011-2012 and compared to observations
29 (Table 2). Despite lower correlations, starting dates in both years and ending dates in 2012 are
30 predicted reasonably well with 38.5, 28.7%, 26.1% of the explained variance. The model
31 however fails in predicting central dates in 2012 with low correlations to experimetally

1 determined dates. Even so the prediction errors of RMSE for all dates in both years are well

2 controlled and the differences between fitting and prediction RMSE are kept within 1.6 days,

3 which means degradation of model performance has limited effects on the prediction of

4 pollen season. Extending the fitting to several years of observation may contribute to improve

5 the stability and robustness of the fitted threshold and further improve the phenology

6 modeling of ragweed.

7

3.3 Model performance and evaluation

9 The evaluation of the model performance is made by comparing the modelled to observed

10 airborne pollen concentrations over the 2000-2010 period. In the Taylor diagram on Fig. 6,

11 we present an overview on how the models perform in terms of spatio-temporal correlations,

12 standard deviations, and RMSEs compared to observations. The statistics are given for

13 different time scales of variability: daily, annual, or for the full 11 years period (in this case, it

14 is equivalent to spatial statistics only). Different variables are analyzed: the daily

15 concentrations, the annual concentration sums, means, and maxima, and the 11 years

16 concentration sum, mean, and maxima. To plot all the statistics on a single diagram, standard

17 deviation and RMSE are normalized by the standard deviation of observations at the relevant

18 spatiotemporal frequency: observations are thus represented by point OBS on the diagram

19 (perfect correlation coefficient, RMSE = 0 and normalized standard deviation =1). The closer

20 a point to the reference OBS, the best is the model skill for this particular variable. From the

21 diagram, we can see that:

22 The model tends to perform very well when the variability is purely spatial and concentrations

23 averages over the 11 year period (dots 5, 6 are very close to OBS). Not surprisingly it means

24 the uncertainties are reduced to a large extent by the calibration procedure. However, the

25 calibrated simulations do not capture the concentration maximum as well and tend to

26 underestimate the measured spatial standard deviation (decade maximum dot 7 and also for

27 the annual maximum dot 4). The model does not perform that well, but still shows some

28 realism when the variability is involved in both spatial and temporal correlations. The yearly

29 statistics, which reflect the interannual variation of pollen concentrations over the stations, are

30 captured well with correlation coefficients all above 0.80 and normalised standard deviations

31 of 0.89, 0.88, and 0.61 for concentration sum, mean, and maximum respectively. When scores

1 are calculated for daily concentrations over all the stations, the overall spatial-temporal

2 correlation coefficient reaches 0.69 for a relative standard deviation of 0.80.

3 Daily variability is obviously the most difficult to simulate but is at the same time the most

4 relevant in term of pollen health impact. To investigate further this point, the model

5 performance is regionally evaluated with both discrete and categorical statistical indicators as

6 listed in Zhang et al. (2012). The discrete indicators considered in this study include

7 correlation coefficient, normalized mean bias factors (NMBF), normalized mean error factors

8 (NMEF), mean fractional bias (MFB), and mean fractional error (MFE). NMBF≤±0.25 and

9 NMEF≤0.35 are proposed by Yu et al. (2006) as a criteria of good model performance.

10 Boylan and Russell (2006) recommended MFB≤±0.30 and MFE≤±0.50 as good performance

11 and MFB≤±0.60 and MFE≤±0.75 as acceptable performance for particulate matter pollution.

12 All metrics are computed over daily time series at each station and on whole European

13 domain (Table 3). For the whole domain, the average values of NMBF, NMEF, MFB, and

14 MFE are -0.11, 0.83, -0.15, and -0.31, respectively. Except for NMEF, the indices fall in the

15 range of good performance according to above criteria. The pollen concentrations over the

16 whole domain are underestimated by a factor of 1.11 based on NMBF. As a measure of

17 absolute gross error, NMEF characterize the spread of the deviation between simulations and

18 observations. Although a relatively large gross error of 0.83 exists, the NMEF obtained here

19 is consistent with what is expected from operational air quality models (Yu et al., 2006;

20 Zhang et al., 2006).

21 The spatial distributions of correlation coefficient, NMBF, NMEF are shown in Fig. 7. The

22 correlations between simulated and observed daily time series are above 0.6-0.7 in the central

23 Europe source region and are mostly above 0.5-0.6 in the source regions of northern Italy and

24 eastern France, while the correlations are low in areas without strong local emission where the

25 majority of observed pollen may originate from long range transport or sporadic ragweed

26 sources. Overall 56.8% of the stations show a NMBF within ±0.25 and 79.5% are within

27 ±0.50. In the source regions of central Europe and eastern France, almost all NMBF values lie

28 within ±0.25. In northern Italy the model mostly overestimates the mean daily pollen

29 concentrations by factors ranging from 1.25 to above 2.0 (except for ITMAGE station).

30 Simultaneous overestimation and underestimation can be found for neighbouring stations,

31 which reflects probably the influence of local and patchy sources difficult to account for at 50

32 km resolution. Better performances are obtained for central European source regions, where

the majority of NMEF are within 1.0. Performance degrades in France, where most NMEF values are within 1.2. Simulations are more problematic over northern Italy, where values of NMEF are often above 1.2. Generally 51.4% of the stations with NMEF are within 1.0 and 79.5% are within 1.4.

A Categorical evaluation is done by classifying the values of pollen concentration with regard to the thresholds of 5, 20, and 50 grains m^{-3}. Hit rates (fraction of correctly simulated exceedances out of all observed exceedances) and false alarm ratio (fraction of incorrectly simulated exceedances out of all simulated exceedances) are calculated from daily time series over the period. On the whole domain, hit rates for these thresholds are 67.9%, 73.3%, and 74.3% and false alarm ratios are 33.3%, 31.9%, and 32.2%, respectively. The model tends to perform better for high threshold exceedance while gives more false alarms for lower threshold. As shown on Fig. 8, there are however large regional differences in model performance. Over central European source region, correct prediction often exceed 80% at moderate and high thresholds and false alarms are about 10% at low and moderate thresholds and 20% at high threshold. Performance degrades in France and northern Italy source regions, where correct predictions are mostly around 50-70% at low and moderate thresholds but false alarms are generally high, especially at moderate threshold.

3.4 Ragweed pollen distribution pattern and risk assessments

With a reasonable confidence in model results, risks region can be identified over the domain. Risk is defined from certain health relevant concentration thresholds: First we can consider minimum ragweed concentrations triggering an allergic reaction. These thresholds are based on experiments involving short exposure time to pollen and then extrapolated in order to define health thresholds in term of daily average concentrations. It is not known, whether a short-time exposure to a large pollen concentration is equivalent to the same dose when less pollen is inhaled over a longer period. Furthermore, these thresholds vary largely between different region and ethnic group. The likely range of such daily thresholds is 5-20 grains m^{-3} per day estimated by Oswalt and Marshall (2008). Very sensitive people can be affected by as few as 1-2 pollen grains m^{-3} per day (Bullock et al., 2012).

On this basis, simulated surface concentrations are post-processed to produce 24-h average concentrations. The footprints of ragweed pollen risk are then obtained by selecting the yearly

1 and monthly maximum from daily averaged concentrations. The yearly and monthly

2 maximums are averaged over the decade (2000-2010) to produce footprints depicted in Figs.

3 9, 10). The risk is divided into 16 levels to reflect the range of health relevant threshold used

4 in different countries and regions as listed in Table 4.3 of Bullock et al. (2012). The numbers

5 of grid cells at different threshold risk levels are given in Table 4. Hereafter we select some of

6 the representative risk levels to be discussed in more details. From annual footprint of

7 ragweed pollen spread risk, the area with concentration ≥ 1 grains m^{-3} occupies almost 50.3%

8 area of domain, with an average concentration of 23.7 grains m^{-3}. The risk pattern extends

9 from European mainland to the seas due to the long-range transport. The lowest risk areas

10 with concentration of 1-5 grains m^{-3} are located over the sea as well as in the countries

11 upwind and far from the known sources, such as Spain, UK, Poland, Belarus, and Latvia. The

12 low risk areas with concentration of 5-20 grains m^{-3} are found on the periphery of the source

13 regions and over Mediterranean Sea, occupying 18.2% of domain. The intermediate risk areas

14 with concentration of 20-50 grains m^{-3} are close to the sources, taking up 6.1% of domain.

15 The areas with very strong stress ≥ 50 grains m^{-3} are concentrated on main sources, taking up

16 5.2% of domain.

17 Temporally, the pollen risk is determined by seasonal evolution (Fig. 10). August is in general

18 the month contributing the most to the annual risk footprint, with an average concentration of

19 25.6 grains m^{-3} (from grid cells with concentration above 1 grains m^{-3}). However for some

20 northern region like Belgium and Germany, the maximum risk is found for September (Fig.

21 10). Overall September shows still important levels 18.9 grains m^{-3} when October and July

22 exhibits much weaker concentrations. The risk areas associated to pollen for each month are

23 given in Table 4.

24 Besides the triggering of allergic reactions at a certain threshold, the time of exposure above a

25 certain threshold might be also important e.g. in term of sensitisation to ragweed pollen. To

26 assess a risk based on this criterion, exposure time, expressed as the decadal average of the

27 number of days per season above a certain threshold, are calculated and reported in Fig. 11.

28 Relevant threshold are 5, 10, 20, 50 grain m^{-3}.

29 The longest exposure times occurs in Pannonian Plain at all thresholds, reaching for example

30 about 30 days above 20 grains m^{-3}. Northern Italy and France can also show some important

31 exposure time. Over the measurement stations, we can compare measured and simulated

32 exposure time at different thresholds as reported in Fig. 11, where measurements are indicated

1   with circles coloured by the measured number of days (left half) and corresponding simulated

2   number of days (right half). Simulated and measured risk agrees reasonably for most stations

3   with in general better comparison for moderate thresholds (10 and 20 grain m^{-3}) relative to

4   high or low thresholds. Nevertheless except for a few stations the simulated exposure time

5   tends to be overestimated.

6

7   4   Summary and conclusions

8   This study presents a regional-climatic simulation framework based on RegCM4 for

9   investigating the dynamics of emissions and transport of ragweed pollen. The RegCM-pollen

10   modelling system incorporates a pollen emission module coupled to CLM4.5 and a transport

11   module as part of the chemistry transport component of RegCM. Because climate, CLM4.5

12   and chemistry components are synchronously coupled to the RegCM model, this approach

13   allows dynamical response of pollen ripening, release, and dispersion to key environmental

14   driver like temperature, photoperiod, soil moisture, precipitation, relative humidity,

15   turbulence, and wind. Through the pollen production link to NPP, other environmental and

16   climate relevant factors as atmospheric CO_2 concentrations are also accounted for. The

17   specific ragweed phenology is parameterized from growth controlled experiment but has to be

18   somehow adjusted to observations for more realism of the flowering season simulations over

19   Europe. Similarly, ragweed spatial distribution is a very poorly constrained parameter which

20   has to be corrected through a calibration procedure. The calibration is performed considering

21   the decadal mean of pollen counts over all sites. As a result the spatial correlation between the

22   simulated and measured average concentrations over the decade is greatly increased (from

23   0.23 to 0.98) by the calibration. While the cross validation aimed at evaluating the calibration

24   shows a corresponding correlation of 0.54 and RESM of 21%, which reflects reasonable error

25   and sensitivity of the calibration. The model measurement correlations based on daily

26   comparison, which are the most relevant for pollen impacts are also increase from 0.28 to

27   0.69. The simulation of daily and interannual variability of pollen concentrations reflect

28   model skills that do not purely rely on the calibration since this one is performed on decadal

29   mean of yearly pollen count.

30   The RegCM-pollen framework is applied to the European domain for the period 2000-2010.

31   Comparing with the observed flowering season, the model can reproduce starting dates and

32   central dates well, with 68.6%, 39.2% of the explained variance and 4.7, 3.9 days of RMSE in

1 starting date and central date, respectively. The pollen season in the main source regions are

2 reproduced fairly well while in the areas with lower ragweed infestation the deviations are

3 evident. The model in generally captures the gross features of the pollen concentrations found

4 in Europe. Statistical measures of NMBF, MFB, and MFE over the domain fall in the range of

5 recommendation for a good performance while NMEF is a bit large with a value of 0.83. The

6 model performs better over the central European source region, where the daily correlations at

7 most stations are above 0.6-0.7 and NMEF lie within 1.0. Performance tends to degrade in

8 France and northern Italy. Still, the values of NMEF for pollen simulation are generally

9 consistent with what is expected from operational air quality models for aerosols for example.

10 Categorical evaluation reveals the model tends to give better predictions for high threshold

11 while gives more false alarms for low threshold. A better performance is also shown over the

12 central European source region at all levels, with correct prediction are above 80% and false

13 alarms are within 20%.

14 The multi-annual average footprints of ragweed pollen spread risk are produced from

15 calibration simulations. The pollen plume with concentration $\geq$ 1 grains m^{-3} can reach on the

16 seas far away from European mainland. The risk areas with concentration above 5 grains m^{-3}

17 are around the source and on Mediterranean Sea, occupying total 29.5% of domain. While the

18 areas with very strong stress $\geq$50 grains m^{-3} are confined in narrow source areas. From the

19 seasonal distribution, August in general contributes most to the annual footprint and

20 September shows still important levels. The longest risk exposure time occurs on Pannonian

21 Plain at all thresholds. Northern Italy and France also show some considerable exposure time.

22 The modelling framework presented here allows simultaneous estimation of ragweed pollen

23 risk both for hindcast simulations (including sensitivity studies to different parameters) and

24 for study of potential risk evolution changes under future-climate scenarios as illustrated in

25 Hamaoui-Laguel et al. (2015). Still a long list of uncertainties hinders an accurate estimate of

26 the airborne pollen patterns and risk within presented framework. Also caution should be

27 taken while interpreting the results in areas without a dense observational network and where

28 calibration is weaker. In this regard, challenging research efforts should focus on a better

29 characterization of ragweed spatial distributions and biomass, in addition, a better

30 understanding of phenological process and the dynamic response of release rate to

31 meteorological conditions will help to reduce these uncertainties and improve model

32 performance. A accurate and diverse observation of ragweed phenology is thererfore of the

essence to better represent local flowering and also there is a need for experimental observations to better constrain the release model. In parallel, systematic ragweed pollen concentrations should be further developed as part of air quality networks and public access to data should be promoted.

Acknowledgements

References

Allard, H. A.: Flowering behaviour and natural distribution of the eastern ragweeds (Ambrosia) as affected by length of day, Ecology, 26, 387-394, 1945.

Boylan, J. W., and Russell, A. G.: PM and light extinction model performance metrics, goals, and criteria for three-dimensional air quality models, Atmos Environ, 40, 4946-4959, doi:10.1016/j.atmosenv.2005.09.087, 2006.

Bullock, J. M., Chapman, D., Schafer, S., Roy, D., Girardello, M., Haynes, T., Beal, S., Wheeler, B., Dickie, I., Phang, Z., Tinch, R., Čivić, K., Delbaere, B., Jones-Walters, L., Hilbert, A., Schrauwen, A., Prank, M., Sofiev, M., Niemelä, S., Räisänen, P., Lees, B., Skinner, M., Finch, S., and Brough, C.: Assessing and controlling the spread and the effects of common ragweed in Europe, Final Report ENV.B2/ETU/2010/0037, European Commission, 456 pp., 2012.

Burbach, G. J., Heinzerling, L. M., Röhnelt, C., Bergmann, K.-C., Behrendt, H., and Zuberbier, T.: Ragweed sensitization in Europe - GA(2)LEN study suggests increasing prevalence, Allergy, 64, 664-665, doi:10.1111/j.1398-9995.2009.01975.x, 2009.

Cecchi, L., Morabito, M., Domeneghetti, M. P., Crisci, A., Onorari, M., and Orlandini, S.: Long distance transport of ragweed pollen as a potential cause of allergy in central Italy, Ann Allerg Asthma Im, 96, 86-91, doi:10.1016/S1081-1206(10)61045-9, 2006.

Chapman, D. S., Haynes, T., Beal, S., Essl, F., and Bullock, J. M.: Phenology predicts the native and invasive range limits of common ragweed, Global Change Biol, 20, 192-202, doi:10.1111/Gcb.12380, 2014.

Chauvel, B., Dessaint, F., Cardinal-Legrand, C., and Bretagnolle, F.: The historical spread of Ambrosia artemisiifolia L. in France from herbarium records, J Biogeogr, 33, 665-673, doi:10.1111/j.1365-2699.2005.01401.x, 2006.

D'Amato, G., Cecchi, L., Bonini, S., Nunes, C., Annesi-Maesano, I., Behrendt, H., Liccardi, G., Popov, T., and Van Cauwenberge, P.: Allergenic pollen and pollen allergy in Europe, Allergy, 62, 976-990, doi:10.1111/j.1398-9995.2007.01393.x, 2007.

Dahl, A., Strandhede, S.-O., and Wihl, J.-A.: Ragweed – An allergy risk in Sweden?, Aerobiologia, 15, 293-297, doi:10.1023/A:1007678107552, 1999.

Deen, W., Hunt, L. A., and Swanton, C. J.: Photothermal time describes common ragweed (Ambrosia artemisiifolia L.) phenological development and growth, Weed Sci, 46, 561-568, 1998a.

Deen, W., Hunt, T., and Swanton, C. J.: Influence of temperature, photoperiod, and irradiance on the phenological development of common ragweed (Ambrosia artemisiifolia), Weed Sci, 46, 555-560, 1998b.

Deen, W., Swanton, C. J., and Hunt, L. A.: A mechanistic growth and development model of common ragweed, Weed Sci, 49, 723-731, doi:10.1614/0043-1745(2001)049[0723:AMGADM]2.0.CO;2, 2001.

Efstathiou, C., Isukapalli, S., and Georgopoulos, P.: A mechanistic modeling system for estimating large-scale emissions and transport of pollen and co-allergens, Atmos Environ, 45, 2260-2276, doi:10.1016/j.atmosenv.2010.12.008, 2011.

Emanuel, K. A., and Zivkovic-Rothman, M.: Development and evaluation of a convection scheme for use in climate models, J Atmos Sci, 56, 1766-1782, 1999.

Fumanal, B., Chauvel, B., and Bretagnolle, F.: Estimation of pollen and seed production of common ragweed in France, Ann Agr Env Med, 14, 233-236, 2007.

Galán, C., Smith, M., Thibaudon, M., Frenguelli, G., Oteros, J., Gehrig, R., Berger, U., Clot, B., and Brandao, R.: Pollen monitoring: minimum requirements and reproducibility of analysis, Aerobiologia, 30, 385-395, 10.1007/s10453-014-9335-5, 2014.

Gallinza, N., Barić, K., Šćepanović, M., Goršić, M., and Ostojić, Z.: Distribution of invasive weed Ambrosia artemisiifolia L. in Croatia, Agriculturae Conspectus Scientificus, 75, 75-81, 2010.

García-Mozo, H., Galán, C., Belmonte, J., Bermejo, D., Candau, P., Díaz de la Guardia, C., Elvira, B., Gutiérrez, M., Jato, V., Silva, I., Trigo, M. M., Valencia, R., and Chuine, I.: Predicting the start and peak dates of the Poaceae pollen season in Spain using process-based models, Agr Forest Meteorol, 149, 256-262, doi:10.1016/j.agrformet.2008.08.013, 2009.

Giorgi, F., Pal, J. S., Bi, X., Sloan, L., Elguindi, N., and Solmon, F.: Introduction to the TAC special issue: The RegCNET network, Theor Appl Climatol, 86, 1-4, doi:10.1007/s00704-005-0199-z, 2006.

Giorgi, F., Coppola, E., Solmon, F., Mariotti, L., Sylla, M. B., Bi, X., Elguindi, N., Diro, G. T., Nair, V., Giuliani, G., Turuncoglu, U. U., Cozzini, S., Güttler, I., O'Brien, T. A., Tawfik, A. B., Shalaby, A., Zakey, A. S., Steiner, A. L., Stordal, F., Sloan, L. C., and Brankovic, C.: RegCM4: model description and preliminary tests over multiple CORDEX domains, Clim Res, 52, 7-29, doi:10.3354/cr01018, 2012.

Grell, G. A.: Prognostic Evaluation of Assumptions Used by Cumulus Parameterizations, Mon Weather Rev, 121, 764-787, doi:10.1175/1520-0493(1993)121<0764:PEOAUB>2.0.CO;2, 1993.

Guenther, A. B., Jiang, X., Heald, C. L., Sakulyanontvittaya, T., Duhl, T., Emmons, L. K., and Wang, X.: The Model of Emissions of Gases and Aerosols from Nature version 2.1 (MEGAN2.1): an extended and updated framework for modeling biogenic emissions, Geosci Model Dev, 5, 1471-1492, doi:10.5194/gmd-5-1471/2012, 2012.

Hamaoui-Laguel, L., Vautard, R., Liu, L., Solmon, F., Viovy, N., Khvorostyanov, D., Essl, F., Chuine, I., Colette, A., Semenov, M. A., Schaffhauser, A., Storkey, J., Thibaudon, M., and Epstein, M. M.: Effects of climate change and seed dispersal on airborne ragweed pollen loads in Europe, Nature Clim. Change, 5, 766-771, doi:10.1038/nclimate2652, 2015.

Helbig, N., Vogel, B., Vogel, H., and Fiedler, F.: Numerical modelling of pollen dispersion on the regional scale, Aerobiologia, 20, 3-19, doi:10.1023/B:AERO.0000022984.51588.30, 2004.

Hirst, J. M.: An Automatic Volumetric Spore Trap, Ann Appl Biol, 39, 257-265, 1952.

Holtslag, A. A. M., De Bruijn, E. I. F., and Pan, H.-L.: A high-resolution air-mass transformation model for short-range weather forecasting, Mon Weather Rev, 118, 1561-1575, DOI: 10.1175/1520-0493(1990)118<1561:AHRAMT>2.0.CO;2, 1990.

Hurtt, G. C., Frolking, S., Fearon, M. G., Moore, B., Shevliakova, E., Malyshev, S., Pacala, S. W., and Houghton, R. A.: The underpinnings of land-use history: three centuries of global gridded land-use transitions, wood-harvest activity, and resulting secondary lands, Global Change Biol, 12, 1208-1229, doi:10.1111/j.1365-2486.2006.01150.x, 2006.

Jäger, S., Mandroli, P., Spieksma, F., Emberlin, J., Hjelmroos, M., Rantio-Lehtimaki, A., and Al, E.: News, Aerobiologia, 11, 69-70, 1995.

Jato, V., Rodriguez-Rajo, F. J., Alcázar, P., De Nuntiis, P., Galán, C., and Mandrioli, P.: May the definition of pollen season influence aerobiological results?, Aerobiologia, 22, 13-25, doi:10.1007/s10453-005-9011-x, 2006.

Karrer, G., Skjøth, C. A., Šikoparija, B., Smith, M., Berger, U., and Essl, F.: Ragweed (Ambrosia) pollen source inventory for Austria, Science of The Total Environment, 523, 120-128, doi:10.1016/j.scitotenv.2015.03.108, 2015.

Kazinczi, G., Béres, I., Pathy, Z., and Novák, R.: Common ragweed (Ambrosia artemisiifolia L.): a review with special regards to the results in Hungary: II. Importance and harmful effect, allergy, habitat, allelopathy and beneficial characteristics., Herbologia, 9, 93-117, 2008.

Martin, M. D., Chamecki, M., and Brush, G. S.: Anthesis synchronization and floral morphology determine diurnal patterns of ragweed pollen dispersal, Agr Forest Meteorol, 150, 1307-1317, doi:10.1016/j.agrformet.2010.06.001, 2010.

Meleux, F., Solmon, F., and Giorgi, F.: Increase in summer European ozone amounts due to climate change, Atmos Environ, 41, 7577-7587, doi:10.1016/j.atmosenv.2007.05.048, 2007.

Oleson, K. W., Lawrence, D. M., Bonan, G. B., Drewniak, B., Huang, M., Koven, C. D., Levis, S., Li, F., Riley, W. J., Subin, Z. M., Swenson, S. C., Thornton, P. E., Bozbiyik, A., Fisher, R., Heald, C. L., Kluzek, E., Lamarque, J.-F., Lawrence, P. J., Leung, L. R., Lipscomb, W., Muszala, S., Ricciuto, D. M., Sacks, W., Sun, Y., Tang, J., and Yang, Z.-L.: Technical description of version 4.5 of the Community Land Model (CLM), NCAR Technical Note NCAR/TN-503+STR, National Center for Atmospheric Research, Boulder, Colorado, 434 pp., 2013.

Oswalt, M. L., and Marshall, G. D.: Ragweed as an example of worldwide allergen expansion, Allergy Asthma Clin. Immunol., 4, 130–135, doi:10.1186/1710-1492-4-3-130, 2008.

Pal, J. S., Small, E. E., and Eltahir, E. A. B.: Simulation of regional-scale water and energy budgets: Representation of subgrid cloud and precipitation processes within RegCM, Journal of Geophysical Research Atmospheres, 105, 29579-29594, doi:10.1029/2000JD900415, 2000.

Pal, J. S., Giorgi, F., Bi, X., Elguindi, N., Solmon, F., Rauscher, S. A., Gao, X., Francisco, R., Zakey, A., Winter, J., Ashfaq, M., Syed, F. S., Sloan, L. C., Bell, J. L., Diffenbaugh, N. S., Karmacharya, J., Konaré, A., Martinez, D., da Rocha, R. P., and Steiner, A. L.: Regional climate modeling for the developing world: the ICTP RegCM3 and RegCNET, B Am Meteorol Soc, 88, 1395-1409, doi:10.1175/BAMS-88-9-1395, 2007.

Payne, W. W.: The morphology of the inflorescence of ragweeds (Ambrosia-Franseria: Compositae), American Journal of Botany, 50, 872-880, doi:10.2307/2439774, 1963.

Pinke, G., Karácsony, P., Czúcz, B., and Botta-Dukat, Z.: Environmental and land-use variables determining the abundance of Ambrosia artemisiifolia in arable fields in Hungary, Preslia, 83, 219-235, 2011.

Prank, M., Chapman, D. S., Bullock, J. M., Belmonte, J., Berger, U., Dahl, A., Jager, S., Kovtunenko, I., Magyar, D., Niemela, S., Rantio-Lehtimaki, A., Rodinkova, V., Sauliene, I., Severova, E., Sikoparija, B., and Sofiev, M.: An operational model for forecasting ragweed pollen release and dispersion in Europe, Agr Forest Meteorol, 182, 43-53, doi:10.1016/j.agrformet.2013.08.003, 2013.

Rogers, C. A., Wayne, P. M., Macklin, E. A., Muilenberg, M. L., Wagner, C. J., Epstein, P. R., and Bazzaz, F. A.: Interaction of the onset of spring and elevated atmospheric CO2 on ragweed (Ambrosia artemisiifolia L.) pollen production, Environmental Health Perspectives, 114, 865-869, doi:10.1289/ehp.8549, 2006.

Shalaby, A. K., Zakey, A. S., Tawfik, A. B., Solmon, F., Giorgi, F., Stordal, F., Sillman, S., Zaveri, R. A., and Steiner, A. L.: Implementation and evaluation of online gas-phase chemistry within a regional climate model (RegCM-CHEM4), Geosci Model Dev, 5, 741-760, doi:10.5194/gmd-5-741-2012, 2012.

Shrestha, A., Roman, E. S., Thomas, A. G., and Swanton, C. J.: Modeling germination and shoot-radicle elongation of Ambrosia artemisiifolia, Weed Sci, 47, 557-562, 1999.

Šikoparija, B., Skjøth, C. A., Radišić, P., Stjepanivić, B., Hrga, I., Apatini, D., Martinez, D., Páldy, A., Ianovici, N., and Smith, M.: Aerobiology data used for producing inventories of invasive species, in: Proceedings of the international symposium on current trends in plant protection, Belgrade, Serbi, 8 September 2012, 7–14, 2012.

Šikoparija, B., Skjøth, C. A., Kübler, K. A., Dahl, A., Sommer, J., Grewling, Ł., Radišić, P., and Smith, M.: A mechanism for long distance transport of Ambrosia pollen from the Pannonian Plain, Agr Forest Meteorol, 180, 112-117, doi:10.1016/j.agrformet.2013.05.014, 2013.

Simard, M. J., and Benoit, D. L.: Effect of repetitive mowing on common ragweed (Ambrosia Artemisiifolia L.) pollen and seed production, Ann Agr Env Med, 18, 55-62, 2011.

Simard, M. J., and Benoit, D. L.: Potential pollen and seed production from early- and late-emerging common ragweed in corn and soybean, Weed Technol, 26, 510-516, 2012.

Skjøth, C. A.: Integrating measurements, phenological models and atmospheric models in aerobiology, Ph.D. thesis, Copenhagen University and National Environmental Research Institute, Denmark, 123 pp., 2009.

Skjøth, C. A., Smith, M., Šikoparija, B., Stach, A., Myszkowska, D., Kasprzykf, I., Radišić, P., Stjepanović, B., Hrga, I., Apatini, D., Magyar, D., Páldy, A., and Ianovici, N.: A method for producing airborne pollen source inventories: An example of Ambrosia (ragweed) on the Pannonian Plain, Agr Forest Meteorol, 150, 1203-1210, doi:10.1016/j.agrformet.2010.05.002, 2010.

Smith, M., Skjøth, C. A., Myszkowska, D., Uruska, A., Puc, M., Stach, A., Balwierz, Z., Chlopek, K., Piotrowska, K., Kasprzyk, I., and Brandt, J.: Long-range transport of Ambrosia pollen to Poland, Agr Forest Meteorol, 148, 1402-1411, doi:10.1016/j.agrformet.2008.04.005, 2008.

Smith, M., Cecchi, L., Skjøth, C. A., Karrer, G., and Šikoparija, B.: Common ragweed: A threat to environmental health in Europe, Environ Int, 61, 115-126, doi:10.1016/j.envint.2013.08.005, 2013.

Sofiev, M., Siljamo, P., Ranta, H., and Rantio-Lehtimäki, A.: Towards numerical forecasting of long-range air transport of birch pollen: theoretical considerations and a feasibility study, Int J Biometeorol, 50, 392-402, doi:10.1007/s00484-006-0027-x, 2006.

Sofiev, M., Siljamo, P., Ranta, H., Linkosalo, T., Jaeger, S., Rasmussen, A., Rantio-Lehtimaki, A., Severova, E., and Kukkonen, J.: A numerical model of birch pollen emission and dispersion in the atmosphere. Description of the emission module, Int J Biometeorol, 57, 45-58, doi:10.1007/s00484-012-0532-z, 2013.

Sofiev, M., Berger, U., Prank, M., Vira, J., Arteta, J., Belmonte, J., Bergmann, K. C., Chéroux, F., Elbern, H., Friese, E., Galan, C., Gehrig, R., Khvorostyanov, D., Kranenburg, R., Kumar, U., Marécal, V., Meleux, F., Menut, L., Pessi, A. M., Robertson, L., Ritenberga, O., Rodinkova, V., Saarto, A., Segers, A., Severova, E., Sauliene, I., Siljamo, P., Steensen, B. M., Teinemaa, E., Thibaudon, M., and Peuch, V. H.: MACC regional multi-model ensemble simulations of birch pollen dispersion in Europe, Atmos. Chem. Phys., 15, 8115-8130, 10.5194/acp-15-8115-2015, 2015.

Solmon, F., Giorgi, F., and Liousse, C.: Aerosol modelling for regional climate studies: application to anthropogenic particles and evaluation over a European/African domain, Tellus B, 58, 51-72, doi:10.1111/j.1600-0889.2005.00155.x, 2006.

Solmon, F., Elguindi, N., and Mallet, M.: Radiative and climatic effects of dust over West Africa, as simulated by a regional climate model, Clim Res, 52, 97-113, doi:10.3354/cr01039, 2012.

Stach, A., Smith, M., Skjøth, C. A., and Brandt, J.: Examining Ambrosia pollen episodes at Poznan (Poland) using back-trajectory analysis, Int J Biometeorol, 51, 275-286, doi:10.1007/s00484-006-0068-1, 2007.

Storkey, J., Stratonovitch, P., Chapman, D. S., Vidotto, F., and Semenov, M. A.: A process-based approach to predicting the effect of climate change on the distribution of an invasive allergenic plant in Europe, Plos One, 9, doi:10.1371/journal.pone.0088156, 2014.

Taramarcaz, P., Lambelet, C., Clot, B., Keimer, C., and Hauser, C.: Ragweed (Ambrosia) progression and its health risks: will Switzerland resist this invasion?, Swiss Med Wkly, 135, 538-548, 2005.

Thibaudon, M., Šikoparija, B., Oliver, G., Smith, M., and Skjøth, C. A.: Ragweed pollen source inventory for France – The second largest centre of Ambrosia in Europe, Atmos Environ, 83, 62-71, doi:10.1016/j.atmosenv.2013.10.057, 2014.

Thornton, P. E., Law, B. E., Gholz, H. L., Clark, K. L., Falge, E., Ellsworth, D. S., Golstein, A. H., Monson, R. K., Hollinger, D., Falk, M., Chen, J., and Sparks, J. P.: Modeling and measuring the effects of disturbance history and climate on carbon and water budgets in evergreen needleleaf forests, Agr Forest Meteorol, 113, 185-222, doi:10.1016/S0168-1923(02)00108-9, 2002.

Thornton, P. E., Lamarque, J. F., Rosenbloom, N. A., and Mahowald, N. M.: Influence of carbon-nitrogen cycle coupling on land model response to CO2 fertilization and climate variability, Global Biogeochem Cy, 21, doi 10.1029/2006gb002868, 2007.

Tummon, F., Solmon, F., Liousse, C., and Tadross, M.: Simulation of the direct and semidirect aerosol effects on the southern Africa regional climate during the biomass burning season, J Geophys Res-Atmos, 115, doi:10.1029/2009JD013738, 2010.

Willemsen, R. W.: Effect of stratification temperature and germination temperature on germination and induction of secondary dormancy in common ragweed seeds, Am. J. Bot., 62, 1-5, doi:10.2307/2442073, 1975.

Yu, S. C., Eder, B., Dennis, R., Chu, S.-H., and Schwartz, S. E.: New unbiased symmetric metrics for evaluation of air quality models, Atmos Sci Lett, 7, 26-34, doi:10.1002/asl.125, 2006.

Zakey, A. S., Solmon, F., and Giorgi, F.: Implementation and testing of a desert dust module in a regional climate model, Atmos Chem Phys, 6, 4687-4704, doi:10.5194/acp-6-4687-2006, 2006.

Zhang, R., Duhl, T., Salam, M. T., House, J. M., Flagan, R. C., Avol, E. L., Gilliland, F. D., Guenther, A., Chung, S. H., Lamb, B. K., and VanReken, T. M.: Development of a regional-scale pollen emission and transport modeling framework for investigating the impact of climate change on allergic airway disease, Biogeosciences, 11, 1461-1478, doi:10.5194/bg-11-1461-2014, 2014.

Zhang, Y., Liu, P., Queen, A., Misenis, C., Pun, B., Seigneur, C., and Wu, S.-Y.: A comprehensive performance evaluation of MM5-CMAQ for the Summer 1999 Southern Oxidants Study episode- Part II: Gas and aerosol predictions, Atmos Environ, 40, 4839-4855, doi:10.1016/j.atmosenv.2005.12.048, 2006.

Zhang, Y., Bocquet, M., Mallet, V., Seigneur, C., and Baklanov, A.: Real-time air quality forecasting, part I: History, techniques, and current status, Atmos Environ, 60, 632-655, doi:10.1016/j.atmosenv.2012.06.031, 2012.

Zink, K., Vogel, H., Vogel, B., Magyar, D., and Kottmeier, C.: Modeling the dispersion of Ambrosia artemisiifolia L. pollen with the model system COSMO-ART, Int J Biometeorol, 56, 669-680, doi:10.1007/s00484-011-0468-8, 2012.

Zink, K., Pauling, A., Rotach, M. W., Vogel, H., Kaufmann, P., and Clot, B.: EMPOL 1.0: a new parameterization of pollen emission in numerical weather prediction models, Geosci Model Dev, 6, 1961-1975, doi:10.5194/gmd-6-1961-2013, 2013.

Table 1. General information (2000-2010) for pollen observation sites. The Annual pollen sum is calculated from 15 July to 31 October. Only years with data available exceeding 67% between 20 July and 2 September are used to determine the observed start date and years with data available exceeding 56% between 3 September and 18 October are used to determine the end date.

Station	city	Country	Longitude	Latitude	Source	Years available (n)	Annual pollen sum (grains m^{-3})	Observed pollen season (Julian day)			Simulated pollen season (Julian day)			RMSEs of pollen season		
								start	centre	End	start	centre	end	start	centre	end
ATPULL	Oberpull	AT	16.504	47.503	EAN	6	656.0	224	243	268	226	242	264	3.6	8.2	0.0
ATWIEN	Vienna	AT	16.350	48.300	EAN	11	1607.7	227	247	276	230	248	276	7.1	4.3	7.6
CHGENE	Geneva	CH	6.150	46.190	EAN	11	200.0	230	243	264	231	243	270	5.2	2.7	10
CHLAUS	Lausanne	CH	6.640	46.520	EAN	11	96.2	231	238	255	232	238	265	5.8	4.1	5.9
DEFREI	Freiburg	DE	7.866	48.000	EAN	11	24.9	239	240	248	236	237	246	2.0	3.0	7.9
AIX	Aix-en-P	FR	5.442	43.535	RNSA	11	238.8	232	243	260	232	245	258	0.0	0.0	0.7
FRANGO	Angouleme	FR	0.164	45.649	RNSA	4	191.5	234	244	256	234	244	255	6.0	3.4	3.4
FRANNE	Annecy	FR	6.133	45.904	RNSA	6	81.3	226	231	247	227	234	256	0.0	0.0	0.0
FRAVIG	Avignon	FR	4.805	43.920	RNSA	6	361.7	230	242	261	230	242	261	5.5	4.1	6.6
FRBESA	Besancon	FR	6.026	47.241	RNSA	6	53.8	239	242	245	244	247	251	0.0	0.0	0.0
FRBOUB	Bourg en B	FR	5.221	46.210	RNSA	5	593.6	229	241	258	229	240	258	5.1	4.2	5.2
FRBOUR	Bourges	FR	2.396	47.084	RNSA	2	300.0	221	236	263	227	238	267	10.0	0.7	0.7
FRCHAL	Chalon S S	FR	4.845	46.780	RNSA	6	252.6	229	241	256	229	240	257	2.7	3.7	4.1
FRCLER	Clermont-F	FR	3.094	45.759	RNSA	6	251.8	236	244	256	235	243	256	5.8	2.8	5.6
FRDIJO	Dijon	FR	5.066	47.319	RNSA	6	134.7	236	246	255	238	247	257	7.9	1.2	6.1
LYON	Lyon	FR	4.825	45.728	RNSA	11	1528.1	222	240	264	224	242	266	4.0	5.3	5.1
FRMONT	Montlucon	FR	2.606	46.344	RNSA	6	197.4	235	243	257	234	242	256	5.9	3.1	4.9
FRNEVE	Nevers	FR	3.161	46.987	RNSA	6	834.2	225	242	261	226	241	261	2.7	1.9	6.6
FRNIME	Nimes	FR	4.350	43.833	RNSA	6	157.3	236	245	258	236	244	258	2.2	3.3	6.4
FRORLE	Orleans	FR	1.898	47.908	RNSA	3	21.3									
ROUSSILLON	Roussillon	FR	4.812	45.371	RNSA	9	5210.2	221	242	262	223	242	263	3.3	3.1	8.0

TOULON	Toulon	FR	5.978	43.127	RNSA	11	133.6	238	246	251	238	243	254	2.5	2.0	0.0
FRTOUS	Toulouse	FR	1.454	43.559	RNSA	6	56.2	245	248	256	243	245	254	0.0	0.0	0.0
FRVICH	Vichy	FR	3.434	46.131	RNSA	3	343.0	227	240	259	229	240	261	6.1	2.8	3.7
BJELOVAR	Bjelovar	HR	16.843	45.897	HRTEAM	6	6993.8	221	240	261	222	239	262	2.9	2.5	4.1
DUBROVNIK	Dubrovnik	HR	18.076	42.649	HRTEAM	6	152.8	240	242	257	241	243	265	3.4	2.9	4.3
KARLOVAC	Karlovac	HR	15.542	45.492	HRTEAM	3	5159.0	218	237	256	219	238	260	1.9	1.4	3.8
OSIJEK	Osijek	HR	18.688	45.558	HRTEAM	4	6924.5	218	240	259	219	241	261	3.3	1.7	4.7
SLAVONSKI	Slavonski	HR	18.023	45.154	HRTEAM	3	13964.0	220	240	266	223	242	267	4.2	3.1	8.0
SPLIT	Split	HR	16.299	43.540	HRTEAM	3	281.3	232	249	259	233	254	266	0.7	8.6	5.5
ZADAR	Zadar	HR	15.235	44.107	HRTEAM	4	515.2	232	244	270	234	245	275	3.4	4.1	9.7
HRZAGR	Zagreb	HR	16.000	45.800	EAN	8	4207.5	221	240	262	222	240	263	4.3	1.8	4.5
HUDEBR	Debrecen	HU	21.583	47.533	EAN	11	7275.4	217	240	264	220	240	265	5.0	3.0	8.5
HUGYOR	Győr	HU	17.600	47.667	EAN	11	2976.5	222	241	268	223	242	271	3.3	5.3	9.4
AGORDO	Agordo	IT	12.021	46.284	ARPA-Veneto	3	0.3									
BELLUNO	Belluno	IT	12.200	46.136	ARPA-Veneto	5	1.4									
JESOLO	Jesolo	IT	12.661	45.510	ARPA-Veneto	5	221.6	235	244	262	236	243	264	2.0	2.7	9.8
LEGNAGO	Legnago	IT	11.315	45.185	ARPA-Veneto	5	175.7	231	244	255	231	245	256	1.9	6.2	11.8
ITMAGE	Magenta	IT	8.883	45.466	EAN	4	5584.8	221	242	267	223	244	267	4.0	4.7	6.6
MESTRE	Mestre	IT	12.250	45.480	ARPA-Veneto	5	290.5	234	244	263	234	243	263	5.2	3.4	10.2
ITPARM	Parma	IT	10.310	44.800	EAN	7	244.1	226	240	257	227	240	258	5.7	2.4	6.2
ROVIGO	Rovigo	IT	11.786	45.049	ARPA-Veneto	4	81.0	240	244	250	238	244	250	6.0	3.0	3.5
VERONA	Verona	IT	10.992	45.427	ARPA-Veneto	5	172.4	230	242	255	230	244	257	1.6	6.7	8.3
VICENZA	Vicenza	IT	11.562	45.546	ARPA-Veneto	5	223.1	232	244	260	232	245	262	7.2	4.9	10.8

1   Table 2. Statistical correlation between simulated and observed ragweed pollen season for

2   fitting 2000-2010 and prediction (2011, 2012).

period	Explained variance (%)			RMSE		
	start	centre	end	start	centre	end
2000-2010	68.6	39.2	34.3	4.7	3.9	7.0
2011	38.5	0.03	14.4	6.2	5.0	8.0
2012	28.7	48.0	26.1	6.3	3.4	8.2

3

4

1   Table 3. Model performance on simulation of daily average concentrations for 2000-2010.

discrete statistical indicators			
normalized mean bias factors (NMBF)	-0.11		
normalized mean error factors (NMEF)	0.83		
mean fractional bias (MFB)	-0.15		
mean fractional error (MFE)	-0.31		
correlation coefficient (R)	0.69		
categorical statistical indicators (%)	Threshold (grains m^{-3})		
	5	20	50
Hit rates	67.9	73.3	74.3
false alarm ratio	33.3	31.9	32.2

2

1   Table 4. Percent area with the surface concentration of ragweed pollen at different risk levels,

2   average for 2000-2010.

level	Lower bound of the thresholds/ (grain m^{-3})	Percent area in domain				
		Jul	Aug	Sep	Oct	annual
1	0	99.6	61.1	54.3	92.4	49.7
2	1	0.2	6.8	11.5	2.3	9.1
3	2	0.1	8.8	10.2	2.7	11.7
4	5	0.0	2.5	1.9	0.3	2.1
5	6	0.1	3.1	3.6	0.5	3.8
6	8	0.0	2.1	2.7	0.3	2.9
7	10	0.0	1.0	1.2	0.1	1.3
8	11	0.0	6.8	6.5	0.8	8.1
9	20	0.0	2.6	2.1	0.4	3.5
10	30	0.0	1.3	1.9	0.2	2.6
11	50	0.0	1.2	1.3	0.0	1.6
12	80	0.0	0.4	0.4	0.0	0.6
13	100	0.0	1.1	1.4	0.0	1.4
14	200	0.0	1.0	0.8	0.0	1.2
15	500	0.0	0.2	0.2	0.0	0.3
16	1000	0.0	0.0	0.0	0.0	0.1

3
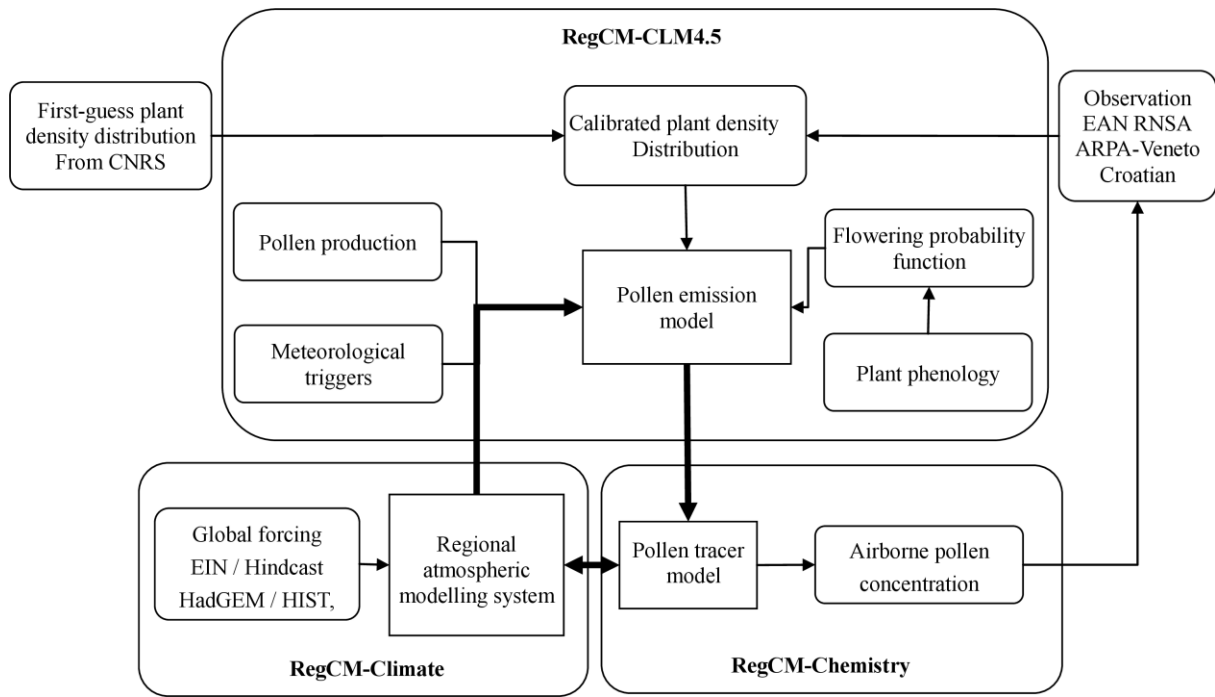
1

2   Figure 1. Ragweed pollen modelling within online RegCM-pollen simulation framework.

3
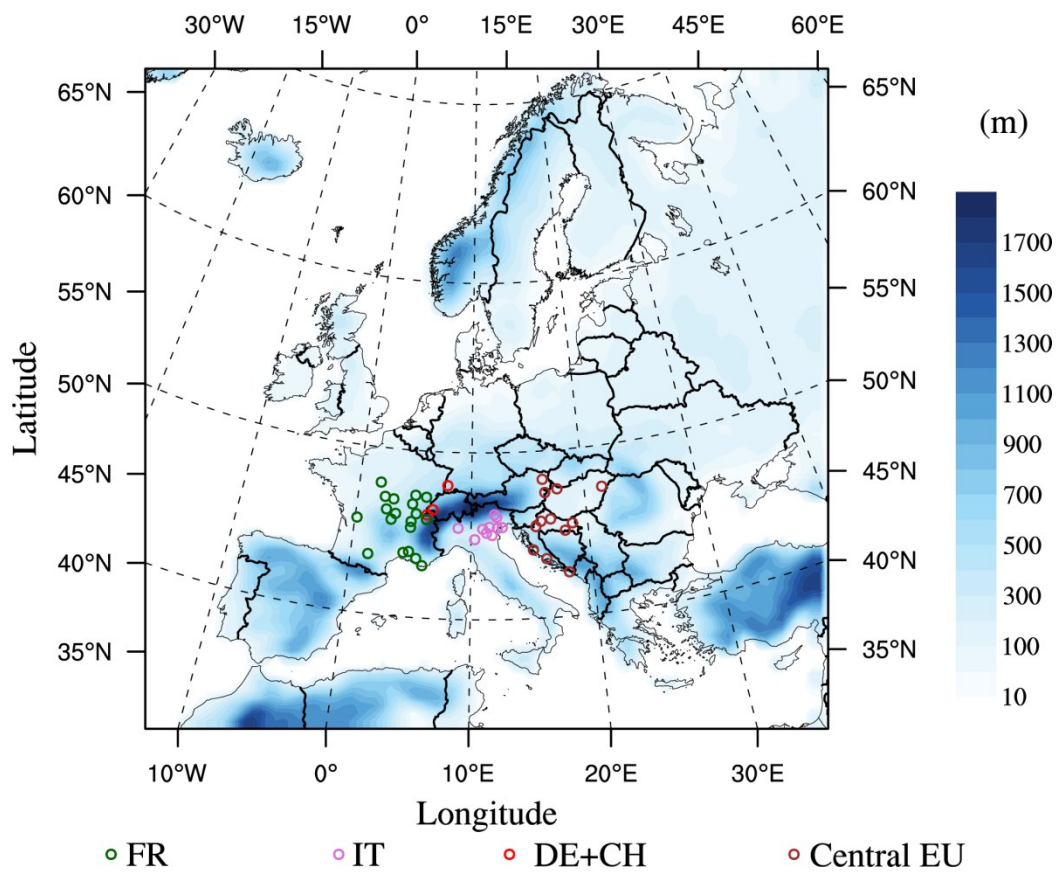
Figure 2. Model domain and the observation sites with topography.
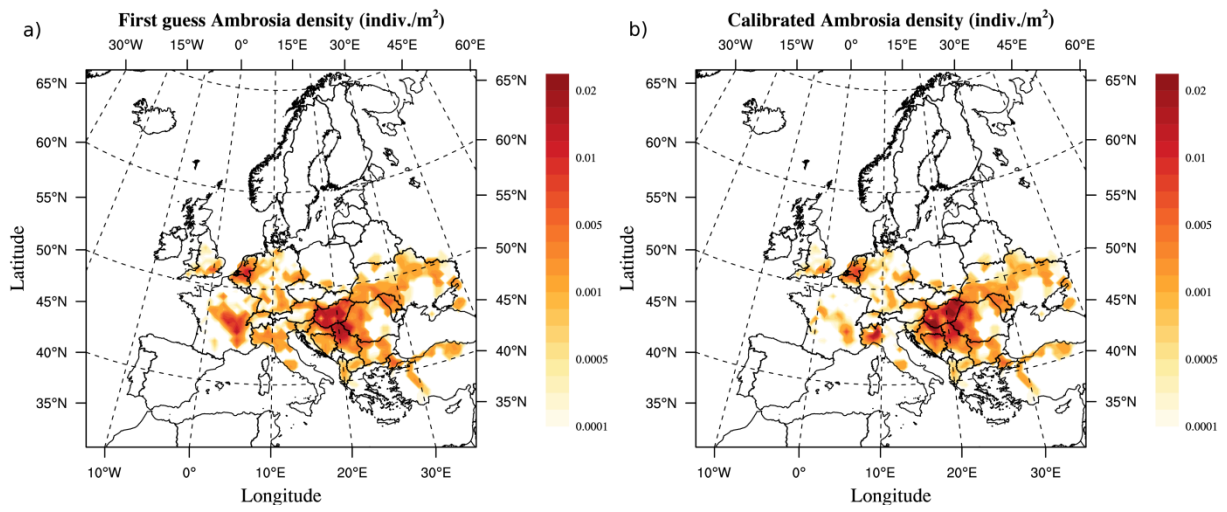
Figure 3. First guess (a) and calibrated (b) ragweed density distribution.
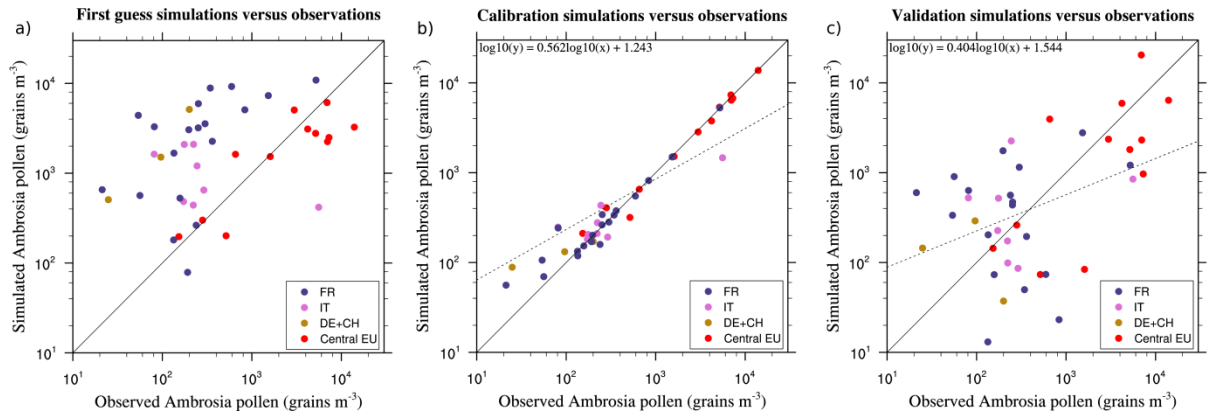
Figure 4. Average (2000-2010) annual pollen sum for first guess (a), calibration (b) and validation (c) simulations on sites.
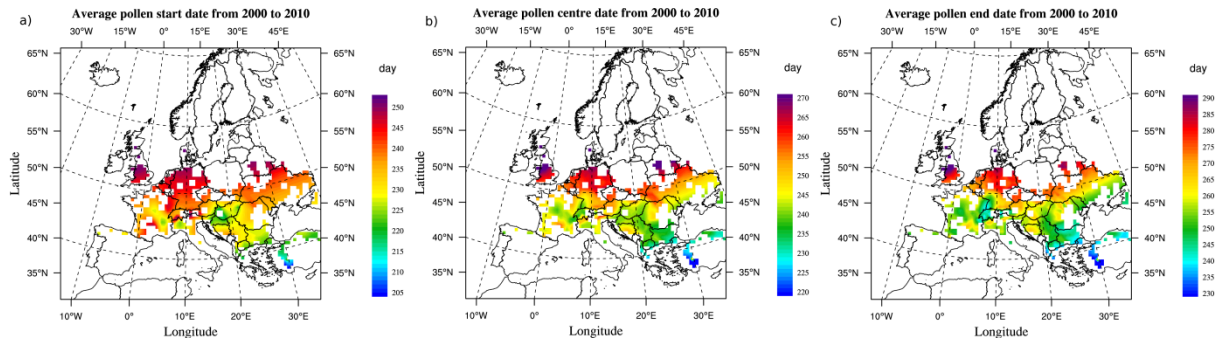
Figure 5. Average pollen season (day of the year) from 2000 to 2010: start dates (a), central date (b), and end dates (c).

1
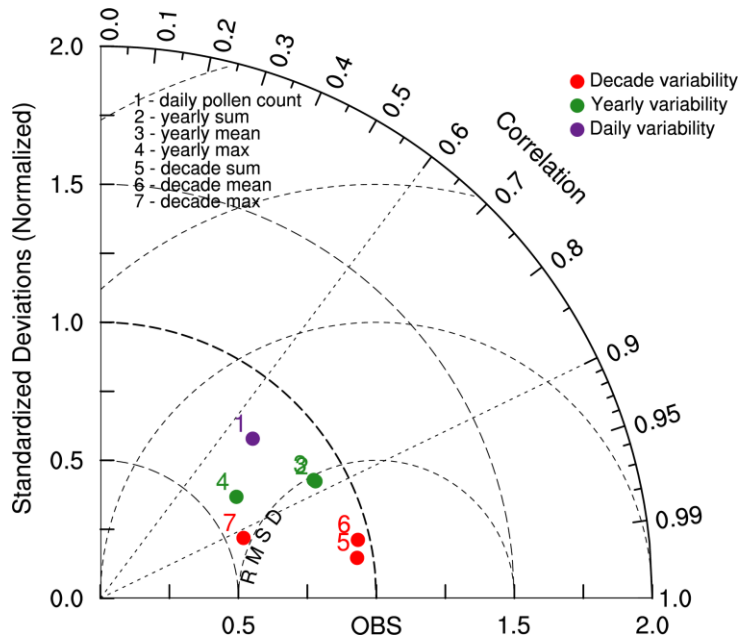
Figure 6. Normalized Taylor diagram showing spatial and temporal correlations coefficients, standard deviations and RMSEs between simulations and observations for the period 2000-2010. Standard deviation and RMSE are normalized by the standard deviation of observations at the relevant spatiotemporal frequency.
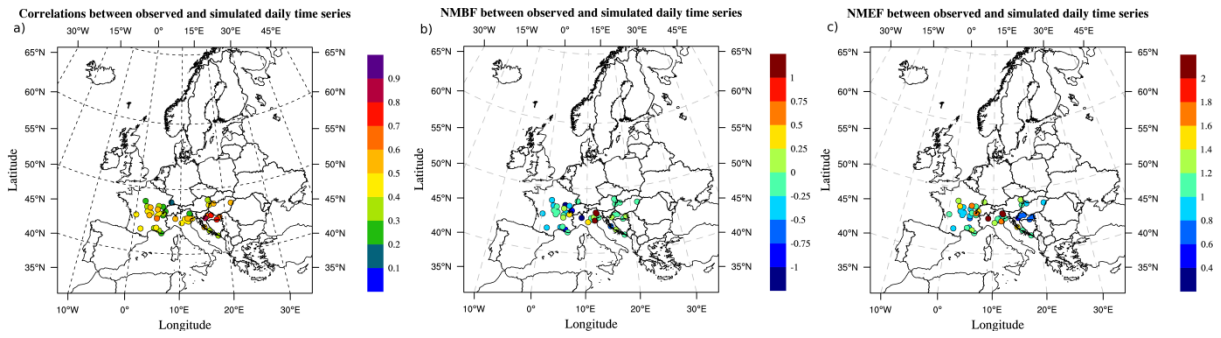
Figure 7. Statistical measures between simulated and observed daily pollen time series for each site: correlation coefficients (a), normalized mean bias factors (b) and normalized mean error factors (c).
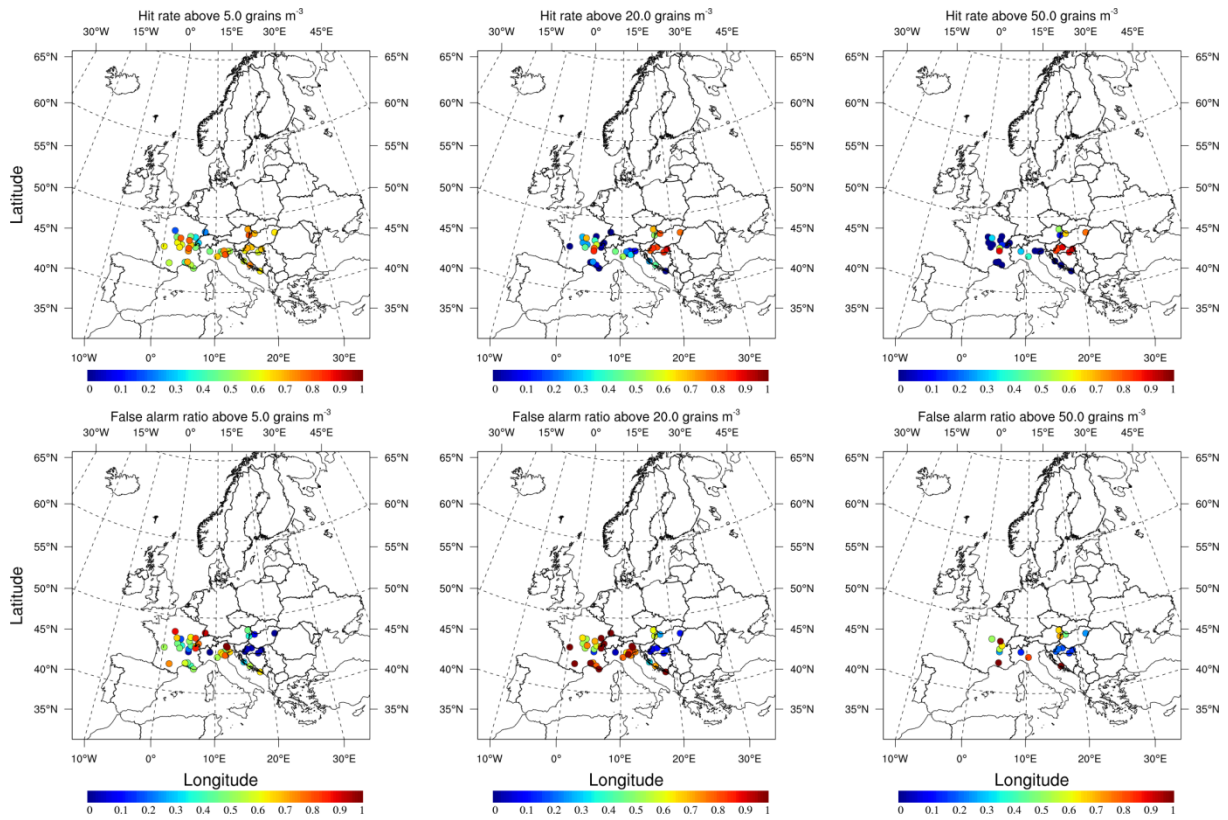
Figure 8. Categorical statistics at thresholds of 5 grains m^{-3} (left column), 20 grains m^{-3} (middle column), and 50 grains m^{-3} (right column): upper panel – hit rate (percentage of correctly predicted exceedances to all actual exceedances), lower panel – false alarm ratio (percentage of incorrectly predicted exceedances to all predicted exceedances).
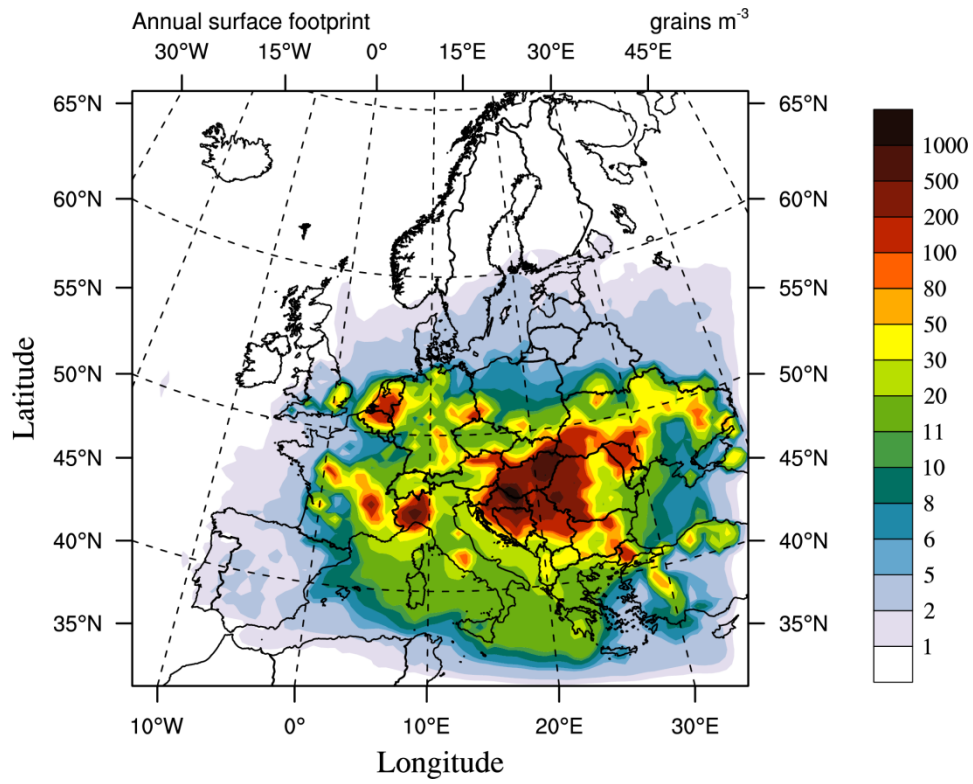
Figure 9. Annual footprint of ragweed pollen at the surface, obtained by selecting the maximum from daily averaged concentrations during the whole pollen season.
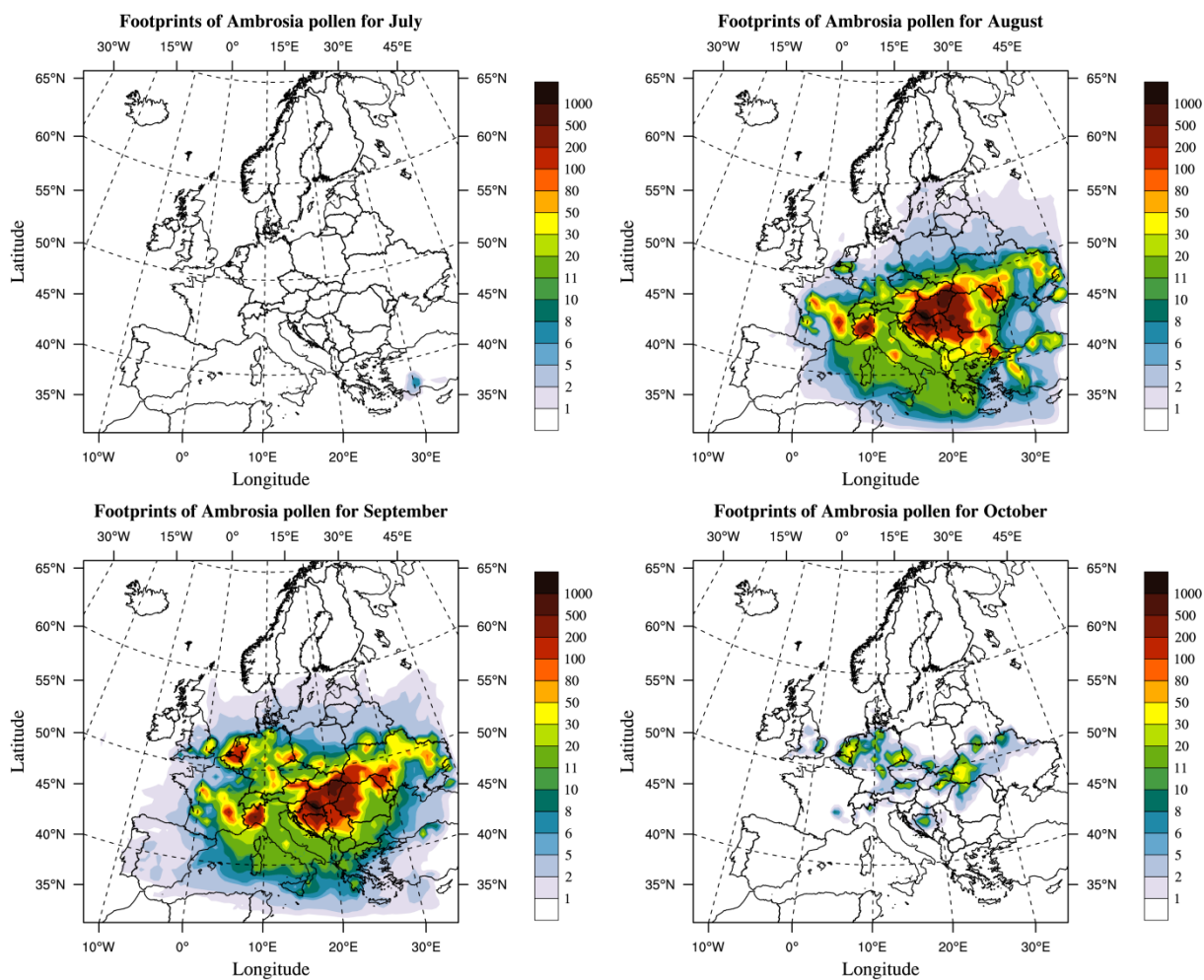
Figure 10. Footprints of ragweed pollen at the surface in each month during pollen season, average from 2000 to 2010, obtained by selecting the maximum from daily averaged concentrations in each month.
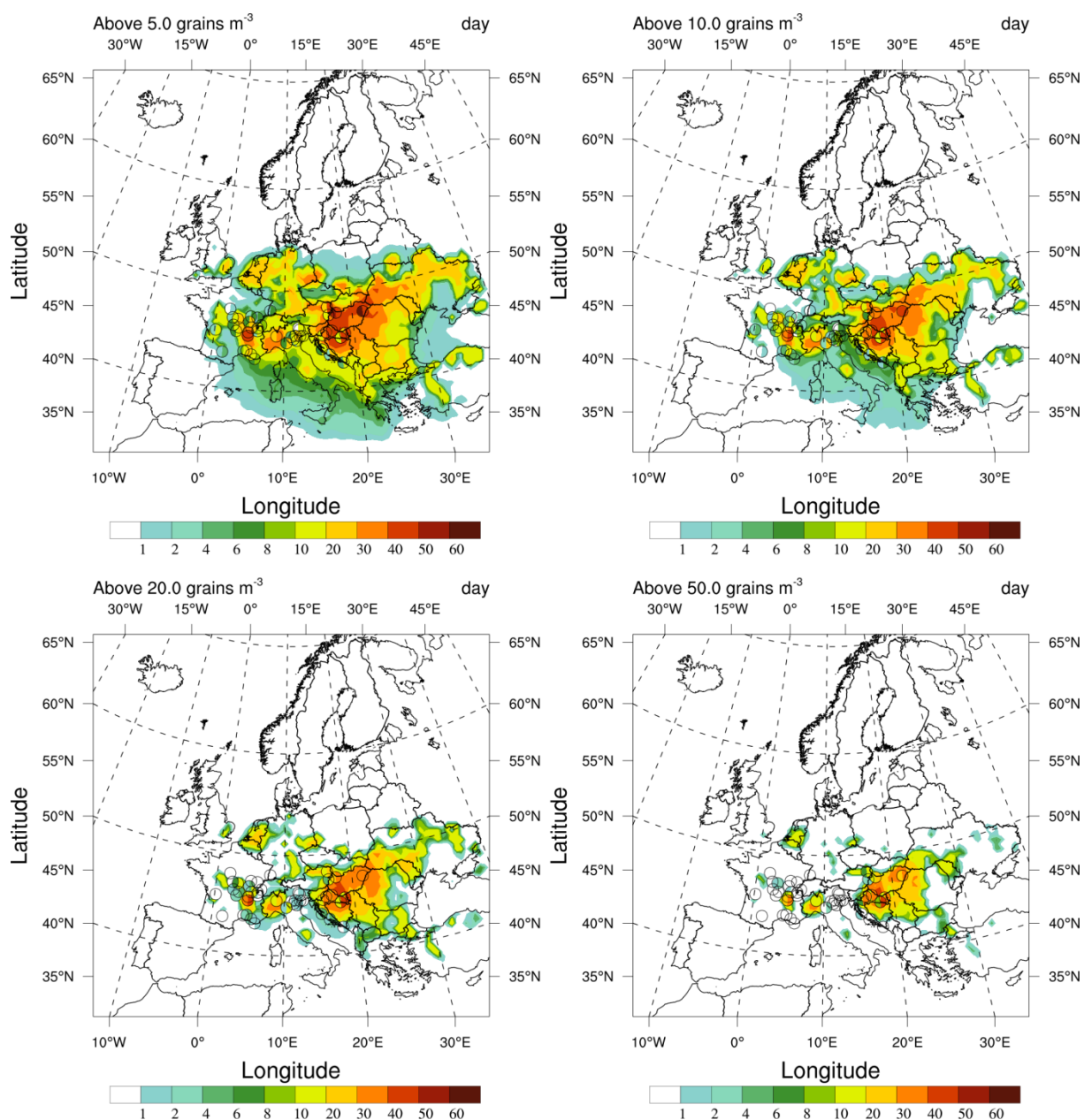
Figure 11. Number of days when the daily average concentration exceeding certain risk levels. Ground-based measurement locations are indicated with circles coloured by the measured number of days (left half) and corresponding simulated number of days (right half).